STUDYING THE MECHANOCHEMISTRY OF BIMOLECULAR REACTIONS USING QUANTUM CHEMICAL SIMULATIONS: ADDITION REACTIONS TO CARBON-CARBON DOUBLE BONDS

by

Benjamin Samuel Carver

A thesis submitted to the Department of Chemistry

In conformity with the requirements for

the degree of Master of Science

Queen's University

Kingston, Ontario, Canada

(November, 2010)

Abstract

Chemical reactions usually involve the conversion of reactants to products by overcoming an energetic barrier. Most commonly, this process can be assisted by adding energy through heat (thermochemistry), light (photochemistry) or electric current (electrochemistry). The fourth option is to overcome the reaction barrier through application of mechanical work, termed mechanochemistry. This method has received much attention from the scientific community in the last decade. Both theoretical and experimental studies have been performed, demonstrating the ability of mechanochemistry to activate reactions, with a strong focus on ring-opening reactions. The vast majority of studies have focused on unimolecular reactions involving bond-rupture, which is very intuitively activated by the application of tensile stress. However, bimolecular reactions, which often involve bond formation as well as rupture, have received much less attention. In this thesis, we seek to change this by undertaking an in-depth study of mechanochemical activation of addition reactions to carbon-carbon double bonds, which involve the formation of two single bonds while the double bond becomes a single bond. We observe that large barrier changes can be induced by applying external force to reactions of this type, and the magnitude of these changes can be controlled by the choice of alkene substrate. By studying the changes induced in the geometry of the substrate, we are able to begin explaining the origins of the barrier reduction effect. In addition, by studying the contributions to the barrier change from mechanical work and the contributions from geometry changes, we discover that steric hindrance to a reaction can play a very significant role in the mechanochemical activation of the reaction.

Acknowledgements

I would like to acknowledge the following people and organizations that made the completion of this thesis possible: My supervisor, Dr. Nick Mosey, for providing me the opportunity to begin working in this fascinating field and the support for me to become successful in it; the following professors for offering advice and assistance throughout my masters research: Dr. Natalie Cann, Dr. Hugh Horton, and Dr. Tucker Carrington; Gurpaul Kocchar, my fellow grad student in the Mosey group for conversations and collaboration on the topic of mechanochemistry; HPCVL and SHARCNET for providing the computational resources necessary for completing these simulations; and finally Queen's University and the Chemistry department for their support both financial and otherwise.

Table of Contents

List of Figures

List of Tables

List of Acronyms

AFM: Atomic Force Microscope

BCB: Benzocyclobutene

CASSCF: Complete Active Space Self Consistent Field

CASMP2: Complete Active Space Moller-Plesset 2nd Order

CCSD(T): Coupled Cluster Singles, Doubles (Triples)

COGEF: Constrained Geometry simulates External Force

DFT: Density Functional Theory

DOF: Degree of Freedom

EFEI: External Force is Explicitly Included

ESR: Electron Spin Resonance

FMPES: Force-Modified Potential Energy Surface

GGA: Generalized Gradient Approximation

LDA: Local Density Approximation

LFP: Link-Functionalized Polymer

NA: Numerical Aperture

PES: Potential Energy Surface

PP: Pulling Point

TMCH: 3,3,6,6-Tetramethylcyclohexene

TS: Transition State

TST: Transition State Theory

QC: Quantum Chemistry

XC: Exchange-Correlation

Chapter 1: Introduction

I. Mechanochemistry

Mechanochemistry is the coupling of mechanical stress and chemical processes at the molecular level. This coupling occurs when a mechanical force deforms a molecular system, whether it be through bond stretching, angle deformation, or rotation of torsions, and this deformation leads to a change in reactivity. Such effects are observed in many chemical reactions. For example, grinding in a mortar breaks the bonds that hold a solid together,[1] and docking a molecule into an enzyme active site stretches and compresses certain parts of the molecule due to electrostatic forces.[2] Both of these processes change how a reaction occurs in the affected molecule and can alter reaction barriers. The change in barriers occurs because applying mechanical force adds energy to a chemical system in the form of work. This work contributes to the energy needed to overcome the reaction barrier and effectively lowers it. A simplified version of this effect can be seen in Figure 1.1, and this concept will be explored in greater detail below. Although the ability of mechanical forces to affect reactions has been observed and employed for millennia, the experimental and theoretical study of these effects has become of great interest only in the past few decades.

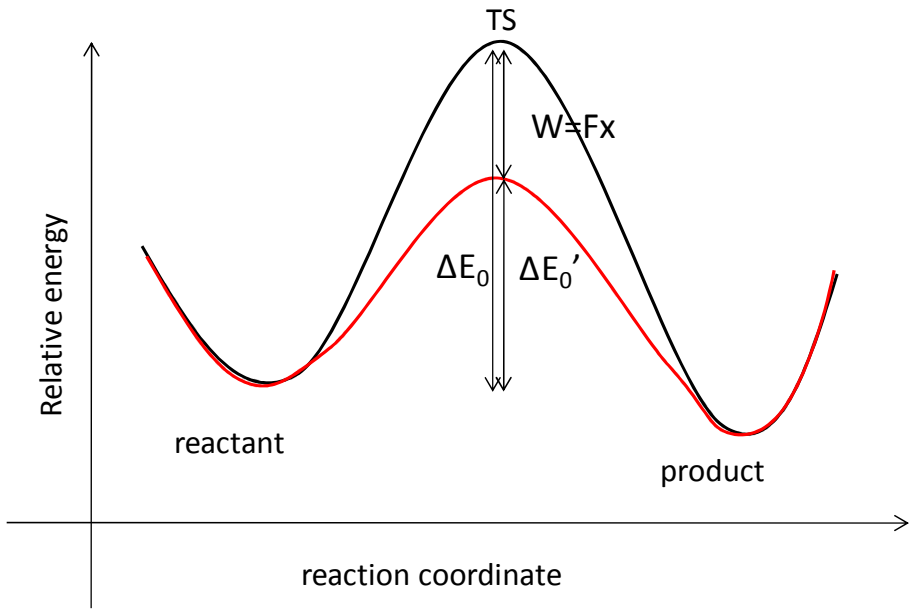

Figure 1.1: A demonstrative plot of the effect of mechanical work on a reaction barrier. By applying a force to the system, the energy of the reactants is increased, thereby decreasing the difference between reactant and transition state energies. Here, ΔE_0 represents the reaction barrier without the addition of an external force; $W=Fx$ is the work done by the force F, and ΔE_0' is the new reaction barrier taking W into account. Thus, the reaction barrier is reduced and this is one of the primary motivations for mechanochemical research. This barrier-reduction phenomenon will be explored in more detail later in this introduction.

The term mechanochemistry has unknown origins, though it is often attributed to Ostwald.[1] Ostwald's textbooks published at the end of the 19th century are generally viewed as the first such books to describe mechanochemistry. The practice, however, has been known since before recorded history. Grinding and milling have long been used by primitive peoples in the preparation of food, pigments, and other solids. The first recorded example of mechanochemistry comes from Theophrastus of Ephesus, a student of Aristotle. [1] He observed that rubbing cinnabar and vinegar together in a brass mortar and pestle yielded metallic mercury, according to the following formula $HgS + Cu \rightarrow CuS + Hg$. This was published in his book *De Lapidibus*, "On Stones," at the end of the fourth century B.C.E. Since this time,

mechanochemistry has been far more rigorously studied in both theoretical and experimental chemistry.

The primary motivation for recent studies of mechanochemistry is the ability of mechanical stress to reduce reaction barriers and selectively guide systems along competing reaction pathways. These abilities offer significant potential in the area of synthetic chemistry. In particular, the mechanical activation and control of unimolecular reactions and reactions occurring in condensed phases have received considerable attention. Studies in these areas employ a wide range of techniques to apply external stresses. These techniques are discussed in part II of this introduction. Part III provides a detailed discussion of experimental studies of mechanochemically-activated reactions. Part IV describes theoretical studies providing additional insight into the effects of applied mechanical stresses on reaction pathways and rates. Part V gives an overview of the application of mechanochemical methods to bimolecular reactions and the potential that still exists in this area. Finally, part VI describes the goals and scope of this thesis.

II. Mechanochemical methods

During the twentieth century, mechanochemistry has found many uses in solid-state chemistry and materials science. Three main types of devices are used for solid-state mechanochemical synthesis.[3] The first kind is a milling apparatus that uses shock action, often involving particles accelerated in a gas jet impacting a solid surface, or by chopping through the bulk system with a moving blade. Examples of these devices include jet mills, turbulent mills and high peripheral-speed pin mills, also called disintegrators. The second type of device uses shear stress, often from rollers. One solid surface moves across another and a substance between

them is exposed to shear forces. The third type, including ball mills, Spex mills, planetary and vibratory mills, uses the same sort of shear mechanism, but usually in conjunction with higher pressures. The pressure-shear force relationship can be varied depending on the specific details of the mill. Milling apparati are able to mechanically activate reactions by increasing both kinetic energy and surface area by physically breaking down solids. This type of activation has seen use in several experiments and syntheses. [4-9]

The methods discussed above are all effective for use with solid materials on a large scale, with sample sizes limited only by the size of the mill. However, these methods are all very nonspecific, with the force applied to the sample lacking specified magnitude or direction. Bond rupture generally occurs at the weakest point in a molecule, but this is not easily predicted. It is difficult using these methods to induce bond rupture elsewhere in the molecule or stop application of force before bonds are broken. In an effort to improve specificity, recent studies in mechanochemistry have focused on the effects of stretching single molecules. The most commonly used methods in this case are atomic force microscopy (AFM), optical tweezers and magnetic tweezers. Diagrams of all of these methods can be seen in Figure 1.2,[10] and Table 1 describes the different force ranges obtainable with these methods.

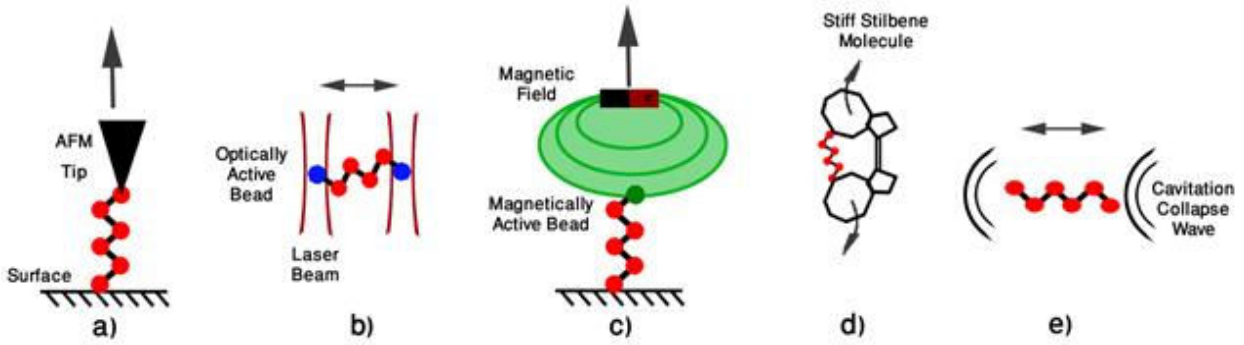

Figure 1.2: Diagrams of the leading methods for single-molecule force microscopy. Image a) represents atomic force microscopy, where a molecule is stretched between a surface and the AFM tip, and force is applied by moving the tip away. Image b) represents optical tweezers, where a bead with a specific refraction index is held at the focal point of a laser beam, and moving the laser will move that bead and a molecule attached to it. The other end of the molecule can either be attached to a surface as in AFM, or to another bead suspended in another laser. Image c) represents magnetic tweezers, where a magnetic bead is held in a magnetic field, and force is applied by moving the magnetic field. Again, the other end of the molecule is attached to a surface. Image d) represents the molecular force probe proposed by Boulatov, where a molecule is attached to both rings of a stiff stilbene or other macrocyclic molecule and force is applied by photoisomerization from cis- to trans-stilbene. Image e) represents sonication, where cavitation bubble collapse creates waves in the sonication solution which induce large-magnitude vibrations in the target molecule.

Table 1: A comparison of methods for applying force to a single molecule. Optical and magnetic tweezers are very precise but limited in the amount of force they can apply. AFM represents the only single-molecule method capable of breaking bonds. MFPs and Sonication trade precision for the ability to affect bulk systems.

Technique	**Force range obtainable (pN)**
Optical Tweezers	0.01-200
Magnetic Tweezers	0.01-100
Atomic Force Microscopy	~3-3000
Molecular Force Probe	150-600
Sonication	<3000

The most popular single molecular manipulation method used in mechanochemistry is atomic force microscopy (AFM). In this method, a sharp tip is used to probe surfaces and molecules attached to surfaces. The tip is attached to a cantilever and deformations in the cantilever can be used to measure the force exerted between the tip and a surface. The typical use of an AFM involves scanning a surface and using the forces measured to determine the

distance between surface and tip as a way to image the surface. In mechanochemistry, the AFM is not used to measure forces, but rather to subject molecules to forces. The typical approach involves bonding one end of a macromolecule to a surface and the other to the tip of the AFM. This approach is demonstrated schematically in Figure 1.2a. Displacing the cantilever extends the macromolecule, which translates into subjecting the molecule to an external force that can facilitate mechanochemical processes.[11] AFMs are able to exert forces in the range from a few piconewtons to a few nanonewtons, which is sufficient to invoke a wide range of mechanochemical processes, including bond rupture.[1, 11]

Optical tweezers are another approach for manipulating individual molecules.[12] A schematic of this approach is given in Figure 1.2b. Optical tweezers, also known as optical traps, are formed by tightly focused laser beams with high numerical aperture (NA). Near the focus of the laser, a dielectric particle is exposed to force from scattering photons. This force has two components: the scattering force, which acts to push a particle in the direction of light propagation, and the gradient force, which acts on a dipole in an inhomogeneous electric field in the direction of the gradient of the field. In the case of an optical trap, the dielectric particle has an instantaneous dipole induced by the laser, and an inhomogeneous electric field is present at the focus, so the gradient force is of relevant magnitude. If the gradient force exceeds the scattering force, the particle is not pushed in the direction of propagation but is trapped at the focal point of the laser. This occurs when the gradient is very steep, as occurs in a highly focused beam from a high-NA objective lens. Due to the balance of gradient and scattering forces, the particle is rarely trapped precisely at the focal point, and is usually found somewhat down-beam from it.[13] Optical tweezers are used in single-molecule force microscopy to stretch polymer molecules when an appropriately dielectric bead is functionalized to one end of the

polymer. This bead can then be manipulated using optical tweezers. In order to stretch a molecule, the other end can also be trapped with optical tweezers or it can be bonded to a surface. Examples involving the use of optical tweezers in the context of mechanochemistry include studying the response of systems such as DNA packaging biomolecules[14] to applied stress and generating motion in several kinds of molecular motors.[15, 16]

Magnetic tweezers have also been used in the context of mechanochemistry. This method is outlined in Figure 1.2c. In a manner analogous to optical tweezers, a magnetic trap can be used to subject molecules to external stresses by placing a magnetic bead at one end of a macromolecule, using either another magnetic trap or a surface anchor at the other end and moving using an electromagnet to elongate the molecule. This method provides direct control over the magnitude and direction of the applied force. The response of several large molecules including DNA,[17] enzymes[18] and lab-on-a-chip microactuators[19] to applied stresses have been studied using this method.

The methods described above can be used to either manipulate bulk materials with little control over the forces applied and bonds affected, or subject individual molecules to precise forces. Individually, none of these approaches is suited to the use of mechanochemistry in the context of practical chemical synthesis, which requires the ability to affect large quantities of molecules using forces that are applied precisely in magnitude, direction and location within the molecule. Recent advances in sonication techniques and the development of molecular force probes have provided this balance between precision and the ability to affect large quantities of molecules. These techniques are discussed below.

Sonication has been increasing in popularity in the past few years as a new method for experimental mechanochemistry. Collapsing cavitation bubbles create waves in the sonication

bath which induce sufficiently large-scale vibrations to cause extension and deformation in affected chemical species, as shown in Figure 1.2e. These effects are localized in time and space and require a threshold amplitude in the activating pulses, which are characteristic of mechanochemical processes in grinding and milling apparati. In the region of cavitation collapse, particle motion reaches several kilometres per second, with temperatures of up to 5000 K and pressure in the tens of atmospheres. [20] Most significantly, sonication has been used to exert forces to drive reactive events in a bulk solution, rather than being used strictly to observe rupture force behaviour.

An alternative means of subjecting molecules to external forces utilizes a molecular force probe (Figure 1.2d).[21] The basic concept behind the molecular force probe is to use a photoisomerizable molecule as a device for subjecting other molecules to stresses. One example of such a system involves a target molecule connected at each end to the phenyl rings of a stilbene. Irradiation causes cis-trans isomerisation about the central C=C bond of the stilbene, which in turn subjects the target molecule to external stresses. The magnitude of the stress can be controlled by connecting the target molecule to the rings of the probe using linkers of different lengths and chemical composition. This approach has two key benefits. First, it is possible to synthesize and irradiate bulk quantities of the probe-target complex. Second, the anisotropic nature of the probe and ability to modify the linkers provides high precision over the direction and magnitude of the applied force.

III. Applications and Prior Experiments

As described above, many methods exist to promote mechanochemical processes on the bulk scale, single-molecule scale, and in between. All of these methods have been used in multiple experiments to explore the role of mechanochemistry in modifying chemical reactions.[11, 14-19, 21, 22] In some cases, they have been used in the practical synthesis of solid state structures and materials, while in other cases their use is limited to studies seeking to understand the fundamental details underlying mechanochemistry. In this section, a number of applications of mechanochemical methods and interesting experimental results will be presented, to provide context for the results put forth in the body of this thesis.

In solid-state mechanochemistry, milling of solids can lead to different forms of mechanical activation. Milling of zeolites with phosphates activates the aluminum surface to produce aluminum centres that interact readily with the phosphate anions. This has application in the production of phosphate-containing fertilizers.[9] In the case of mechanical milling of platinum compounds, bond-cleavage causes changes in reactivity. For example, Mitchenko *et al* discovered that milling K_2PtX_6, where X is Cl or Br, leads to homolytic cleavage of the Pt-X bond, giving rise to free X_2 molecules.[6] In this experiment, K_2PtX_6 was placed in a vibratory mill, and after 1 hour the system was tested for the presence of X_2. The addition of methyl iodide into the reaction vessel after milling K_2PtCl_2 yields methyl chloride, a reaction which does not occur without the milling step. It is well known that methyl iodide will react with gas phase chlorine to yield methyl chloride, thus indicating that Cl_2 was formed during the milling process. These results were supported with electron-spin resonance experiments.

Other experiments involving mechanochemical activation through milling include extensive work on ferrous spinel, MFe_2O_4, where M is a divalent transition metal cation. Under

milling conditions, bulk samples of spinels are transformed into nanometer-sized crystallites. Further milling yields MO, FeO and metallic iron. Prolonged ball milling has been observed to convert $LiAlH_4$ into a mixture of Al, H_2, and Li_3AlH_6. The metal species were identified by X-ray powder diffraction, and this reaction is believed to be catalyzed by iron contaminants from the mill vessel.

Ball milling of kaolinite, a type of clay, yields interesting results through homolytic bond cleavage.[7] In this process, Si and Al mechanoradicals are created by the milling process and H_2 is observed as a byproduct. H_2 is a common product of the reaction of radicals with H_2O, but in the experiments performed by Kameda[7], no H_2O was present before milling. H_2 could have been produced by reaction of radicals with hydroxyl groups, or molecular H_2O could have been produced by mechanically-promoted proton transfers between these hydroxyl groups. Of particular interest is the fact that H_2 concentration increased as the milling time increased, indicating that radicals continued to be produced up to the maximum studied milling duration of 600 minutes. Milling is also used in the metallurgy industry, where mechanochemical processing and mechanical alloying are both processes involving metal powders being treated in a ball mill; mechanochemical processing induces various chemical reactions while mechanical alloying induces cold fracturing and welding of metals in a similar apparatus.

Much research has been performed regarding the mechanochemistry of polymer solids and rubbers, which are semi-solid macromolecular mixtures. In such compounds, bond cleavage gives rise to radicals that remain localized rather than distributing through a solution, as occurs in polymer liquids. It was observed by Watson that mastication of natural rubber reduced the molecular weights of compounds in the rubber by an order of magnitude.[8] Homolytic bond cleavage giving rise to a pair of free radicals was the predicted mechanism for this degradation,

and experiments with radical-acceptor molecules confirmed this hypothesis.[4, 5] The production of these free radicals can lead to several kinds of reactive events depending on the environment of the masticated rubber, including reactions with molecular oxygen or with other polymer molecules to form block or graft polymers. Electron spin resonance (ESR) experiments have also been used to confirm the creation of radicals by homolytic cleavage in mechanical milling of these compounds. ESR results also show an increase in radical formation with increasing force.[8, 23]

Zhurkov and Korsukov[24] examined the end groups formed by milling of polyethylene and polypropylene solids. Vinyl, vinylene and methyl end groups were formed without the presence of oxygen, and aldehyde functionalities were produced in the presence of oxygen. The formation of these groups was explained based on disproportionation reactions occurring after the mechanically-induced formation of primary radicals. Based on IR spectra taken after different milling times, rates and activation energies for the breakdowns were determined. In addition to ball milling, shear forces and ultrasonic irradiation have been observed to induce homolytic cleavage of the type described above.[1] A study by Porter and Johnson[25] determined that this sort of degradation in polymers stops at an equilibrium value of the polymer molecular weight, which has an inverse linear dependence on the applied force. Mechanical stress has also been observed to cause decreases in the molecular weights of glasses and crystalline solids.

In addition to solid-state experiments, a great number of mechanochemical studies have been performed using AFM.[26-29] The most popular use of AFM has been for binding and rupture force measurements. Grandbois used AFM to measure the rupture force of carboxy-amylose polymers by attaching one end of the polymer to an AFM tip while the other end was covalently bonded to a functionalized glass surface.[26] The polymers were chemically activated and bonded

to amino-functionalized glass, and an amino-functionalized AFM tip was used to pull the polymers. The tip was brought into proximity with the surface in a stepwise fashion and then retracted, an approach called "fly-fishing mode". A distinct event was observed at F= 275 pN which corresponded to a chair-boat inversion of the furanose rings. The peak associated with this event was very sharp when only one polymer was attached, but much broader with multiple attachments. This result is of particular relevance because it represents an observable change in the geometry of the molecule that does not include bond breaking. Though rupture force is measured in this experiment, the chair-boat inversion is clearly apparent and happens well before the bond-rupture event, as shown in Figure 1.3.

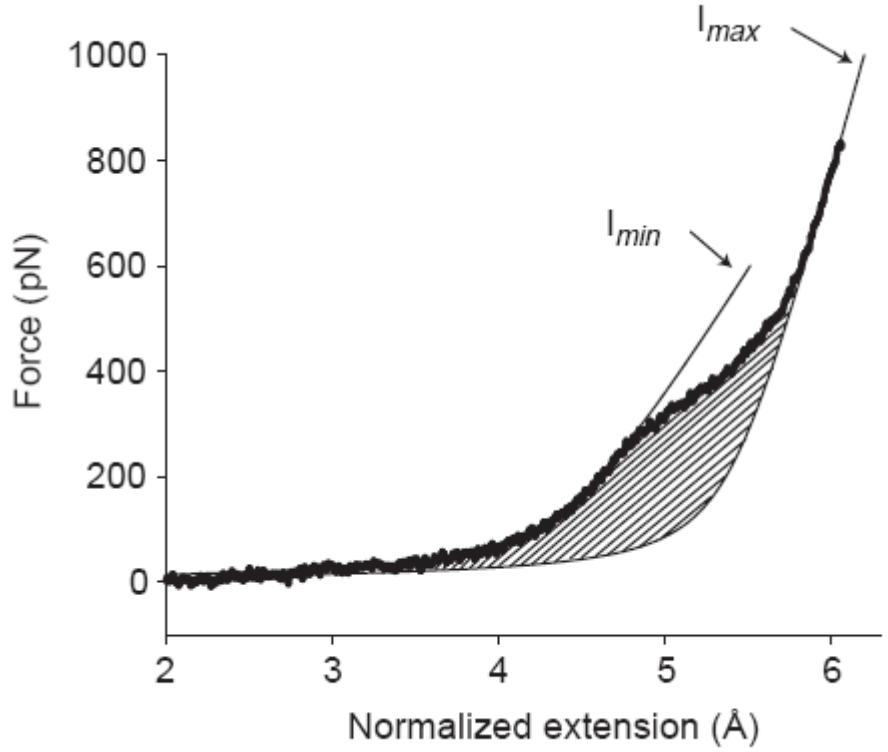

Figure 1.3: A force vs extension curve for carboxy-amylose polymers, showing the plateau region corresponding to a chair-boat inversion of the amylose rings. The thick trace is the experimental result, the thin trace corresponds to a theoretical fit indicating the force vs extension curve that should be seen if the chair-boat inversion did not happen. The hashed area indicates the energy change from having this inversion take place.[26]

Due to the broadening of this inversion event with multiple polymer attachments, it can be used to identify when a single attachment remains. Fly-fishing was employed until a single attachment was detected, after which the AFM tip was retracted until bond rupture was observed. This occurs in several irreversible steps, indicated by many microruptures before the molecule ruptured fully, freeing the tip from the surface. Since these microruptures correspond to length increases in the polymer chain in multiples of the monomer length, it was determined that a number of covalent surface anchors must give way before the molecule breaks completely. The rupture force at 10 nN/s loading rate was determined to be approximately 2 nN. Density Functional Theory (DFT) calculations were used to conclude that the weakest bond in the system, that which ruptures, is the C-Si bond at the surface anchor.[26] The theoretical rupture force for this bond is 2.7 nN, and the lower value obtained experimentally is explained using a combination of temperature and solvent effects which are not included in static gas-phase DFT calculations. A different experiment used amino-thiols on a gold surface to bond to the carboxy-amylose polymer without changing the attachment to the AFM tip. Here, the rupture force was observed to be 1.4 nN, and theoretical calculations by Kruger[30] determined that this corresponds to the surface linkage again, with the pulling of the thiolate molecule leading to a monatomic gold nanowire which ruptures with a force of approximately 1.2 nN.[27]

Similar experiments have also been carried out on metallic bonds, using gold nanowires pulled by AFM. [28, 29] It is well known that pulling on gold atoms at a nanojunction will produce monatomic gold nanowires, so the use of a gold AFM tip brought into contact with a gold surface allows for a straightforward molecular-scale study of metallic bonds. Retracting the gold tip produces a stretched gold nanowire. The electrical conductance of the nanowire was used to judge its diameter, since a single gold atom has a conductance very near the quantum unit of

conductance, $2e^2/h$. The conductance thus provides a measure of the thickness of the wire. Discrete force events were observed whenever tensile force caused the diameter of the wire to shrink by one gold atom, or whenever a new gold atom was pulled out of the surface and added to the wire. In both room-temperature and liquid helium temperature experiments, the rupture force was observed to be 1.5 nN. It is unknown why these values are the same, but the low-temperature results have been supported by computational calculations.[29]

Sonication methods have found extensive use recently in the area of mechanochemistry. A key study involved using sonication to induce the ring-opening of benzocyclobutene (BCB) under mechanochemical conditions.[22] This study is of particular interest because it demonstrates mechanoselectivity. Specifically, the ring-opening of BCB is governed by the Woodward-Hoffmann rules, which dictate that the ring should open along a disrotatory pathway under photochemical conditions and along a conrotatory pathway under thermochemical conditions, as outlined in Figure 1.4. As discussed below, that study demonstrated that the rules could be overcome through the application of mechanical stress.

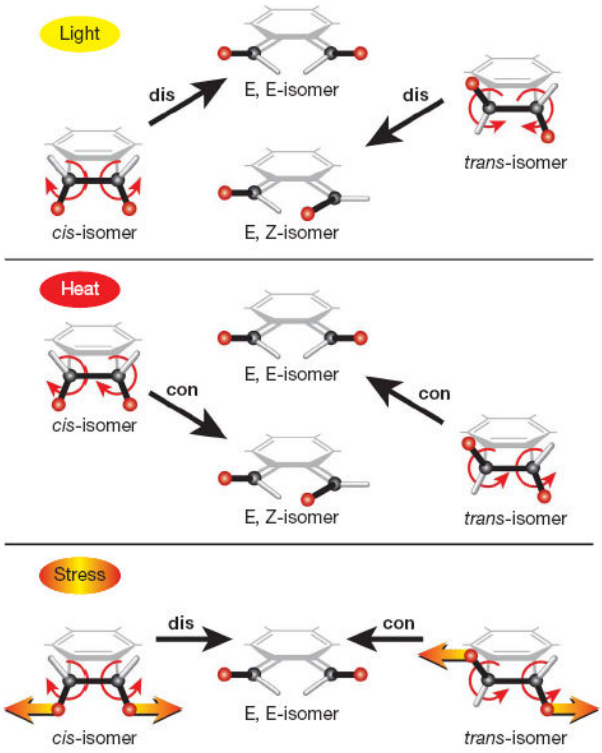

Figure 1.4: Photochemical, thermochemical and mechanochemical ring openings of benzocyclobutene. [22] Under photochemical conditions, ring opening always follows a disrotatory mechanism, and different starting isomers will yield different product isomers. Under thermochemical conditions, ring opening always follows a conrotatory mechanism. Under mechanochemical conditions, ring opening always yields the E,E product isomer and different starting isomers will follow different mechanisms to reach this product.

BCB molecules were incorporated into link-functionalized polymers (LFP) so that one BCB unit would be present at the centre of each polymer of 40 kDa molecular weight as shown in Figure 1.5. These polymers extend and contract under sonication conditions, thus subjecting the scissile bond of BCB to tensile forces. The rupture of this bond yields a diene, which can then undergo a Diels-Alder reaction with N-(1-pyrene)-maleimide. The structure of the product can then be analyzed to determine the arrangement of the polymers in the diene, and hence determine whether BCB opened along conrotatory or disrotatory pathways.

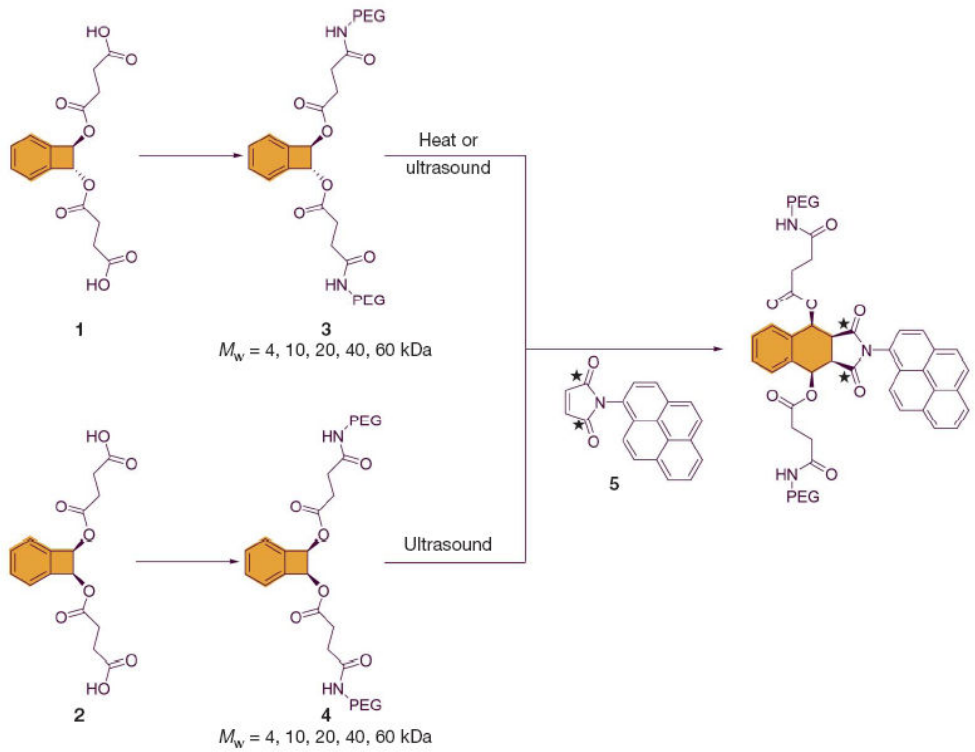

Figure 1.5: Diels-Alder reaction between BCB units in LFPs and a dieneophile which leaves a pyrene tag in the product which can be detected by gel permeation chromatography. [22] BCB is incorporated into a poly(ethylene glycol) LFP, undergoes a ring-opening to form a diene, and then reacts with N-(1-pyrene)-maleimide to yield the structure on the right. This reaction can only occur if the ring-opening yields the E,E-isomer and so the pyrene tag was used to test that under mechanochemical conditions the ring-opening will always yield this product.

The results are summarized in Figure 1.5. Essentially, the study demonstrated that both starting conformers of the BCB polymer yielded the same product under sonication, indicating that both starting conformers yielded the same conformer of the diene after ring-opening. This is in direct opposition to the Woodward-Hoffmann rules, which state that the starting conformer should dictate the ring-opened conformer. This work was of key interest because it demonstrated that mechanical stress can be used to overcome the Woodward-Hoffmann rules, with the choice of con- or disrotatory opening being based on the choice of pulling points, rather than the reaction conditions. More generally, this effect is known as mechanoselectivity: the

product of a reaction under mechanochemical conditions can be selected on the basis of the locations of groups used to subject the molecule to an external force.

Mechanochemical activation has also been examined with molecular force probes. [21] As with sonication, the stilbene probe was used not only to obtain a rupture force, but to mechanically activate a chemical reaction. A paradigmatic unimolecular reaction, the dissociation of a carbon-carbon bond in trans-3,4-dimethylcyclobutene, was found to be accelerated by stretching with this force probe. The target molecule was incorporated into linkers of varying length between the rings in both E and Z isomers of stiff stilbene.[21] The different linker sizes allowed for differing values of restoring force to be observed. Both isomers were allowed to react thermally to obtain kinetic data, and the Z isomers were also irradiated at temperatures too low for thermal reaction. Under irradiation, the presence of the diene product was detected in concentrations dependent on both temperature and photon flux. This was taken to indicate that the C-C dissociation was being activated by the E-Z photoisomerization of the force probe. The restoring force exerted in the linkers was calculated using density functional theory (DFT), and it was found that the enthalpic barrier to the reaction decreases steadily as the applied force was increased by changing the length of the linker. This is illustrated by the data in Figure 1.6.

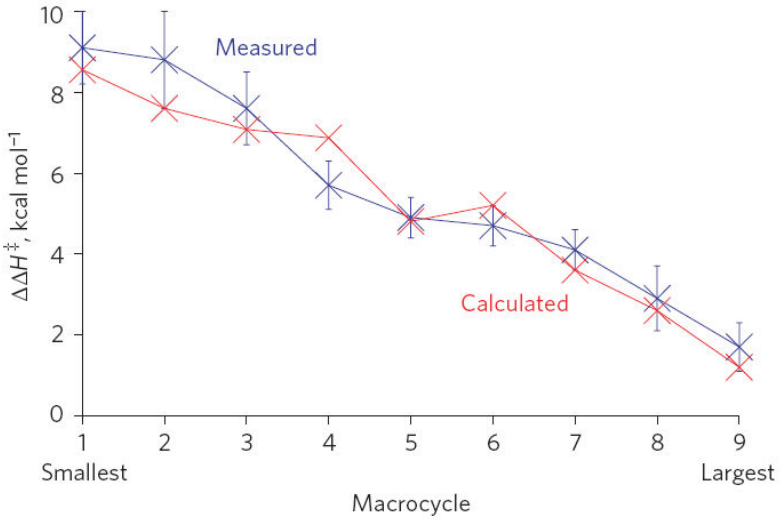

Figure 1.6: Changes in the enthalpic barrier for ring-opening of dimethylcyclobutene as an approximate function of applied force. When using the stiff stilbene force probe, the size of the macrocycle is used to modify the magnitude of the applied force, with larger macrocycles inducing smaller forces. This plot therefore is reversed from those shown in the results section of this thesis, with high values on the x-axis corresponding to low forces and high values on the y-axis corresponding to a large enthalpic barrier change. Thus this Figure demonstrates that high values of applied force as inferred from a small macrocycle size lead to large changes in the enthalpy of reaction, for a large decrease in the reaction barrier.[21]

IV. Theoretical Studies

In addition to experimental studies, a great amount of theoretical work has been performed in the area of mechanochemistry. These studies have been performed using quantum chemical (QC) calculations in conjunction with techniques implemented to perform calculations on a force-modified potential energy surface. The details of these methods are discussed in Chapter 2.

Early theoretical studies of mechanochemical processes focused on evaluating bond rupture forces for a large number of different bonds and demonstrating how bond rupture can be accelerated mechanochemically. [31-33] Research has also been done into studying chemical reactions. Electron transfer processes occurring during bond rupture processes under

mechanochemical conditions have been studied.[34] The results demonstrate that in a protic solvent, stretched polymers break heterolytically; this process is stabilized by the partial positive charge of the solvent molecule over the homolytic bond cleavage more commonly seen in mechanically-induced bond breaking. This study also showed that applied stresses can be used to accelerate hydrolysis reactions.

DFT calculations were also used to evaluate the forces generated by molecular force probes. In the ring-opening experiment performed by Boulatov,[21] geometries for reactants and transition states were calculated for a range of different macrocycles, and also for analogous structures where the cyclobutene ring was removed. It was theorized that the difference in the atomic forces for the structures including the ring and the structures where it was removed would correspond to the forces applied by the strain in the ring. Since the enthalpies obtained from these calculations were similar to those obtained experimentally, it was assumed that the forces would also be accurate.

Other interesting phenomena examined through *ab initio* calculations include a decrease in the cis-trans isomerisation barrier of polyacetylene.[35] This result is especially interesting because it does not involve actual bond rupture, only the reduction of bond order, and thus represents a more gentle application of mechanochemistry.

The circumvention of the Woodward-Hoffmann rules mentioned above has prompted several theoretical studies of the ring-opening of cyclobutene and benzocyclobutene under mechanochemical conditions. Martinez and coworkers[36] used static CASMP2 calculations and first-principles molecular dynamics to study this process and determined that applying external forces across the scissile bond decreases the reaction barriers in a manner that can overcome the Woodward-Hoffmann rules.[36] This is apparent from the data shown in Figure 1.7, and was

confirmed in subsequent calculations by Marx and coworkers. [37] More recent work by Mosey *et al*[38] has shown that applying mechanical stresses does not alter the changes in electronic structure that occur during the ring-opening of cyclobutene. As such, the Woodward-Hoffmann rules are actually violated when the system opens along the disrotatory pathway while remaining on the ground state, where a photochemical ring-opening would require moving to an excited state. However, that study also showed that the orbital effects that disfavour progression along this pathway are rendered secondary to mechanochemical effects, thereby providing a more fundamental explanation for violating the Woodward-Hoffmann rules under mechanochemical conditions.

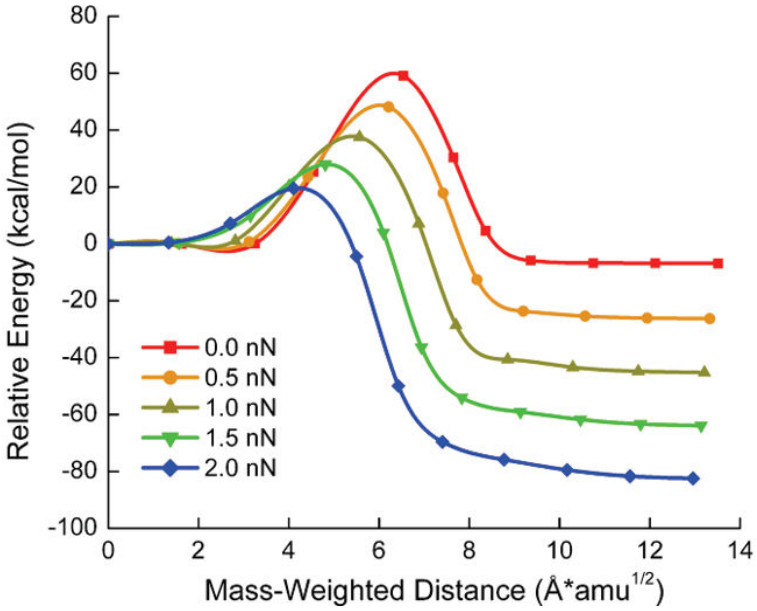

Figure 1.7: Potential energy as a function of reaction coordinate for the mechanically-assisted ring opening of benzocyclobutene at increasing values of applied force. The results demonstrate that increasing the applied force decreases the reaction barrier and shifts the position of the transition state along the reaction coordinate.[36]

V. Mechanochemistry of Bimolecular Reactions

To date, studies of reactions occurring under mechanochemical conditions that do not involve bond rupture, and especially studies of bimolecular reactions, have been rare. The use of

mechanochemistry for bimolecular reactions is less intuitive than for unimolecular reactions such as bond cleavage. In his 2005 review,[34] one of the seminal works on mechanochemistry, Beyer notes the scarcity of work on bimolecular reactions, and devotes less than a page of his 28-page paper to previously published examples. Mechanical work has been observed to favour the ozonization of polypropylene[39, 40] and the hydrolysis of polyamides, which was observed to follow a rate law similar to a modified Arrhenius model.[41] Thermooxidation of polypropylene and polyethylene, on the other hand, was observed to occur more slowly under applied force.[42, 43] These reaction barrier changes have been attributed to more than just addition of energy through mechanical work, however. Changes in the geometry of the system are viewed as a large contributor to the change in rate. Specifically, if mechanical stress induces a geometry change towards the transition state, reaction barriers will decrease, and the opposite is also true. In most bimolecular reactions, bonds form as well as break, so applying forces to stretch bonds does not necessarily lead to activation of such a reaction. Thus, to study such reactions it is necessary to use low forces, where the geometry changes induced are deformations of angles and torsions, and bond-stretching effects are minimal. Figure 1.8 depicts kinds of geometry changes are induced by different approximate values of applied force. Significant changes are seen at far lower forces than the bond-breaking regime. This notion of low-force geometry changes as a key element of barrier reduction is very important to the results presented in this thesis.

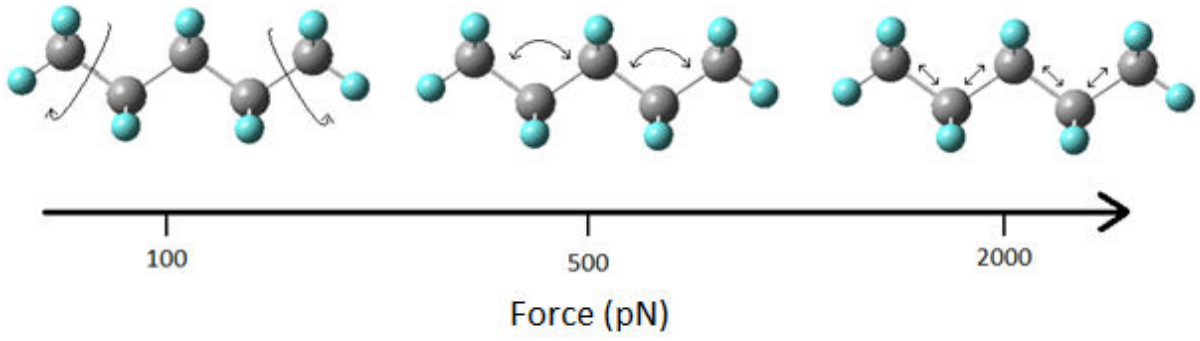

Figure 1.8: Geometric degrees of freedom affected at different values of applied force. Torsion rotations are the weakest degrees of freedom and are affected in the range of a few hundred piconewtons. Forces between this and one nanonewton will begin to deform angles, and in the range of a few nanonewtons, bond distances begin to stretch. These are approximate ranges. The specific value of force needed to affect a specific bond, angle, or torsion will be dependent on the system being studied.

VI. Goals of this Thesis

It has been shown that the regime of bond angle and torsion deformation is the range from 100 to a few hundreds of piconewtons, while the bond-breaking regime is a few nanonewtons.[44] Of the methods in common use, only AFM and sonication have the ability to exert forces in the bond-breaking regime, with the others only capable of a few hundred piconewtons. As a result, it seems valuable to study mechanochemistry in the <1 nanonewton region; that is, the area of angle and torsion deformation. This requires study of chemical processes other than bond rupture, and thus we chose to pursue the relatively unexplored area of the mechanical activation of bimolecular reactions. As discussed above, bond stretching is of the greatest use in unimolecular reactions, whereas bimolecular reactions require the use of smaller forces to affect different degrees of freedom. This approach poses several interesting questions: can these subtle, low-force regime geometry deformations have a significant effect on reaction energies and barriers? If so, what would cause these effects without a large force or bond breaking? Finally and most importantly, how could these effects be applied to synthesis? To

answer these questions, a range of different bimolecular reactions involving carbon-carbon double bonds was studied. Reaction barriers were calculated in an attempt to determine what criteria make a reaction susceptible to mechanical stresses. Changes in the reaction barriers under applied force were broken down into contributions from mechanical work and from molecular energy changes resulting from moving on the Born-Oppenheimer Potential Energy Surface (PES). The goal is to create a model for choosing reactions which will be responsive to techniques such as sonication or molecular force probes for the increase of reaction rates in chemical synthesis.

Chapter 2: Methods - Static Quantum Chemical Calculations

I. Introduction

The results presented in this thesis were all obtained by performing simulations of chemical reactions at the molecular level to observe the effect of applying mechanical force on reaction barriers. In order to do this, accurate geometries of molecules and the associated electronic energies must be determined, and for this we use static quantum chemical (QC) calculations. The specific QC method employed was DFT, and as such this method will be the focus of the discussion in this chapter. I used this method to calculate optimized geometries at both minima and saddle points on the potential energy surface, as well as vibrational frequencies, and the molecular energies associated with all of these structures. This chapter begins with a discussion of mechanochemical methods in QC in Section II. The basics of density functional theory is discussed in Section III, followed by a description in Section IV of the basis sets which can be employed with this method. Section V explains the process of geometry optimization and Section VI describes the determination and use of vibrational frequencies. Finally, Section VII describes the kinetic models used to describe reactions such as those studied in this thesis.

II. Incorporating Mechanical Stress into Quantum Chemical Calculations

Calculations performed under mechanochemical conditions employ the following force-modified potential energy surface (FMPES):

$$E(F, \mathbf{q}) = E_{BO}(\mathbf{q}) - Fx(\mathbf{q}) \quad (1)$$

where $\mathbf{q}$ represents the atomic coordinates, F is the magnitude of an external force applied between two atoms in the molecule used as pulling points, $x(\mathbf{q})$ is the distance between the pulling points, E represents the energy on the force-modified potential energy surface, and E_{BO}

represents the energy on the standard Born-Oppenheimer PES. To perform calculations under mechanochemical conditions, our group has added the ability to calculate equation (1) and use it in the context of exploring PESs into the NWChem[45] and Quantum-Espresso[46] software packages. All calculations reported in this thesis were performed with a modified version of NWChem.

E_{BO} in equation (1) can be obtained from standard QC calculations. Meanwhile, flexibility exists in how to determine and use the work term, $Fx(\mathbf{q})$. Specifically, one can perform calculations in which F is treated as the independent variable and calculating $x(\mathbf{q})$ based on F. This approach is termed External Force is Explicitly Included (EFEI).[37] The alternative approach involves fixing $x(\mathbf{q})$ to a constant value and determining what value of F corresponds to this constrained distance. This technique is called COnstrained Geometry simulates External Force (COGEF).[31] A comparison of how force is applied with these two methods is shown in Figure 2.1. Figure 2.2 shows the effect on the energetics of a stretched bond using EFEI. The data in this Figure show how the application of an external force can significantly alter the energetics associated with chemical processes. Furthermore, the data show that the equilibrium bond length is not significantly affected by the application of force, with this distance increasing by only ~0.1 Å with an applied force of 3 nN. The curve shapes for COGEF would be similar, but the magnitude of the changes for each value of applied force would be different. This shows the specific energy changes induced in a system by specific values of applied force.

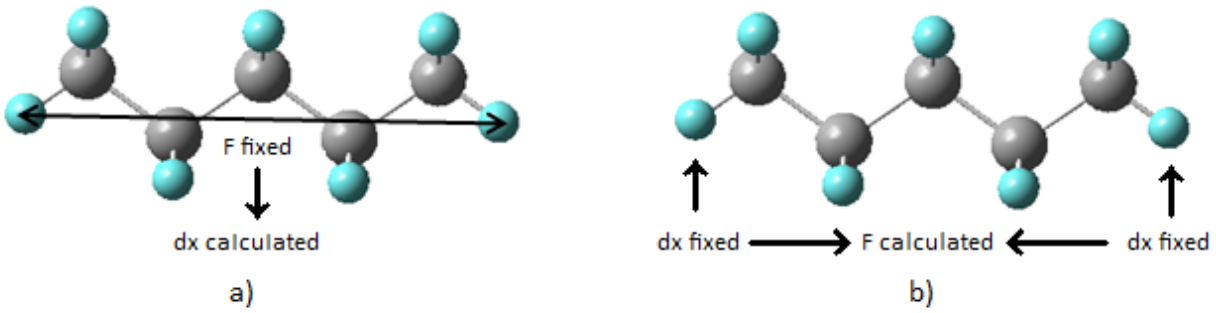

Figure 2.1: Differences in application of force between (a) EFEI and (b) COGEF. The same pulling points are used in both molecules. To apply an EFEI force, the vector between the two pulling points is calculated, and the force is applied along this vector. From this, we obtain a geometry with a new distance between the pulling points. To apply a COGEF force, the distance between the pulling points is fixed. From this, the force between the two pulling points can be calculated. Thus, EFEI uses a force to obtain a geometry and COGEF uses a geometry to obtain a force.

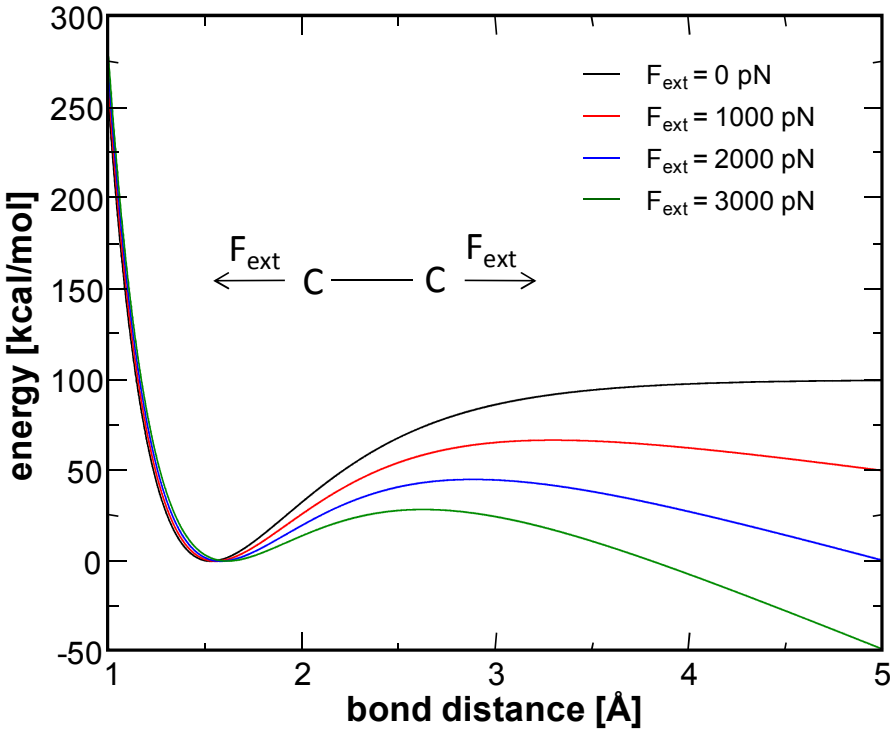

Figure 2.2: Energy vs bond length curves for varying values of *F* applied using EFEI. In this case, a C-C single bond is approximated by a Morse potential. From these curves the effects of force on the energetics of an elongated bond can be seen. The energy at large bond distances is very clearly affected in a manner that will accelerate bond dissociation. Meanwhile, the equilibrium bond distance is not significantly altered with increasing force.

Up until 2009, all published calculations of mechanochemical processes used COGEF. [31-35, 47] In 2003, this method was used to measure the changes in proton affinity of dimethyl ether under mechanochemical conditions.[34] This property can be determined by the difference in potential energy between an elongated molecule of dimethyl ether and the corresponding elongated protonated molecule. The results demonstrated that the proton affinity increased with elongation (larger external force), illustrating the ability to model mechanochemical processes with the COGEF method. However, that study also illustrated deficiencies in COGEF. Specifically, in order to compare energies of different structures with COGEF, those structures must be exposed to the same F. Controlling F is not straightforward when treating $x(\mathbf{q})$ as an independent variable. To do this, it is necessary to perform calculations of the products and reactants for a large range of $x(\mathbf{q})$, evaluate E versus $x(\mathbf{q})$ curves for each system, differentiate these curves with respect to $x(\mathbf{q})$ to obtain F and then take the differences in the energies of the system at the points where the values of F are the same. This is illustrated in Figure 2.3 and represents a major impediment to the practical application of the COGEF method.

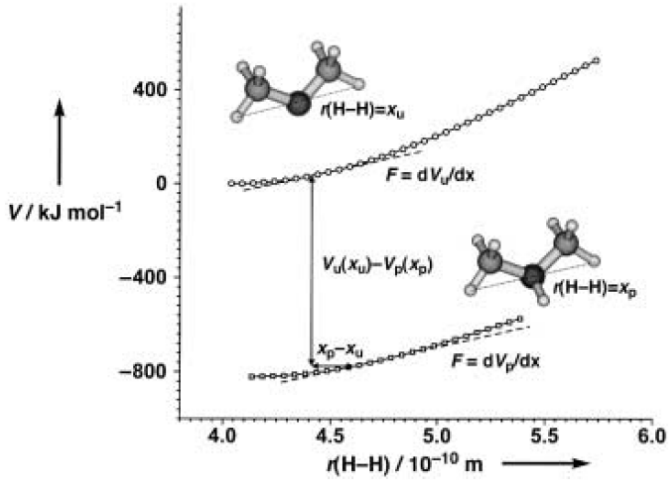

Figure 2.3: Calculation of proton affinity as a function of force using COGEF.[34] Potential energy is determined as a function of extension for both protonated and unprotonated dimethyl ether, and force is calculated as the first derivative of this curve. Proton affinity is then defined as the difference between these two potential energy curves at points where the first derivatives are the same. Thus, to express proton affinity as a function of force requires performing this calculation at many different points along the V vs r(H-H) curves.

In addition to technical inconveniences, the COGEF method suffers from the fact that it does not treat *F* as the independent variable. Recent work by Marx has demonstrated that this is necessary to properly describe chemical systems under mechanochemical conditions.[37] That work led to the development of the EFEI approach discussed above. The EFEI model naturally lends itself to studies of mechanochemical reactions and readily sheds light on the origin of mechanochemical effects. For example, the barrier to a chemical reaction is expressed within the EFEI formalism as:

$$\Delta E^{\ddagger}_{EFEI} = \Delta E^{\ddagger}_{BO} - F\Delta x \qquad (2)$$

Here, $\Delta E^{\ddagger}_{EFEI}$ is the change in total barrier, $\Delta E^{\ddagger}_{BO}$ is the change in barrier calculated using geometries on the force-modified Born-Oppenheimer PES, *F* is the applied force as in equation

2, and Δx is the change in x in going from reactant to transition state. A stretching force is defined as positive, so it can be seen that if Δx is positive, a stretching force works to pull the molecule towards its transition state geometry and the barrier decreases. If Δx is negative, a compressive force would be needed to accelerate the reaction, and a stretching force would result in a reaction barrier increase. It should be noted that since EFEI treats force as an independent variable, the calculation of proton affinity as a function of force as attempted by Beyer[34] becomes much simpler. Potential energy versus force curves would be obtained for the protonated and unprotonated molecules, and the value of proton affinity as a function of force would simply be the difference between these curves. The EFEI technique is used in all calculations reported in this thesis.

III. Density Functional Theory

Traditional quantum mechanics allows for the calculation of many molecular properties from solutions of the Schrödinger equation.[48] Until the 1990s, these so-called *ab initio* methods were the standard approach for performing quantum chemical calculations. The most commonly used *ab initio* method is Hartree-Fock, which can be used on its own to calculate molecular properties, and also serves as a starting point for more advanced *ab initio* methods that capture a portion of the electron correlation. In the last twenty years, however, density functional theory (DFT) calculations have surpassed *ab initio* methods as the preferred approach to QC calculations.[49] The underlying rationale is that DFT calculations offer the accuracy provided by post-Hartree-Fock techniques at an expense that is comparable to that of Hartree-Fock.

The underlying principle of DFT is the first Hohenberg-Kohn theorem.[49] This states that all ground state properties of a molecule are functionals of the electron density, which is

itself a function of the spatial coordinates. Among the properties that can be calculated in this way is the electronic energy, which is generally divided into kinetic energy, electron-electron repulsion and electron-nuclear attraction terms as shown in equation 3.

$$E[\rho] = \underbrace{T[\rho]}_{\substack{\text{kinetic energy} \\ \text{of the electrons}}} + \underbrace{E_{\text{Ne}}[\rho]}_{\substack{\text{nuclear-electron} \\ \text{interaction energy}}} + \underbrace{E_{\text{ee}}[\rho]}_{\substack{\text{electron-electron} \\ \text{interaction energy}}} \tag{3}$$

Each of the terms in this equation is a functional of the electron density, which is itself a function of the spatial coordinates as described above. Also it should be noted that while this describes the electronic energy, an internuclear Coulombic repulsion term is necessary to calculate the total molecular energy.

One difficulty with using equation (3) is that the kinetic energy functional of the electron density is unknown. An early attempt at developing a kinetic energy functional used a homogeneous electron gas as a model, but it was found that this functional did not allow for chemical bonding to occur. [49] To rectify the problem, Kohn and Sham suggested obtaining the density from an artificial wavefunction Ψ_s, constructed from a set of noninteracting single-particle orbitals ψ_i. [49] The orbitals in this wavefunction could be used to evaluate the kinetic energy with standard quantum mechanical operators and the other terms in equation (3) could be calculated using the electron density. With this, the molecular energy as a functional of electron density is given by:

$$E[\rho] = \sum_{i=1}^{n_{occ}} \left\langle \psi_i \left| \frac{-\nabla^2}{2} \right| \psi_i \right\rangle + E_{\text{Ne}}[\rho] + E_{\text{ee}}[\rho] \tag{4}$$

where the terms on the left side of this equation are, in order, the kinetic energy of the electronic system, the electron-nuclear interaction term and the electron-electron interaction term. With such a system, the electron density can be calculated as follows:

$$\rho(\mathbf{r}) = \sum_{i}^{n_{occ}} |\psi_i(\mathbf{r})|^2 \tag{5}$$

Treating all nuclei as point charges according to the Born-Oppenheimer approximation gives the nuclear-electron term as:

$$E_{\mathrm{Ne}}[\rho] = -\sum_{\mathrm{I}} \int \frac{Z_{\mathrm{I}}\rho(\mathbf{r})}{|\mathbf{R}_{\mathrm{I}} - \mathbf{r}|} d\mathbf{r} \tag{6}$$

where the index I covers all nuclei, with Z_I representing the nuclear charge of atom I and $\mathbf{R}_\mathrm{I}$ being its nuclear coordinates. This is a Coulombic attraction relationship.

The last term in equation (3) corresponds to electron-electron interaction, and is divided into two components in the Kohn-Sham DFT formalism. One of these components represents the Coulombic repulsion felt by an electron in an average electric field generated by the other electrons while the other, E_{xc}, is termed the exchange-correlation energy and is one of the biggest challenges to successful DFT calculations. This will be discussed in more detail below.

From the components outlined above, a full expression for the Kohn-Sham electronic energy functional can be assembled.

$$E[\rho] = \sum_{i=1}^{n_{occ}} \langle \psi_i | \frac{-\nabla^2}{2} | \psi_i \rangle - \sum_{I} \int \frac{Z_{\mathrm{I}}\rho(\mathbf{r})}{|\mathbf{R}_{\mathrm{I}} - \mathbf{r}|} d\mathbf{r} + \frac{1}{2} \int\int \frac{\rho(\mathbf{r})\rho(\mathbf{r}')}{|\mathbf{r} - \mathbf{r}'|} d\mathbf{r} d\mathbf{r}' + E_{\mathrm{xc}}[\mathrm{p}] \tag{7}$$

Solving this equation requires the determination of a wavefunction that minimizes the total energy while maintaining the number of electrons in the system and the orthogonality of the approximate orbitals. To do this, the self-consistent field approach used in Hartree-Fock is employed, but the details of this process are beyond the scope of this document. The first three terms of this expression can be calculated in a straightforward manner once the orbitals are known. The fourth term, the exchange-correlation term, is not as easy to elucidate, and the

expression used for this term is one of the main ways to tune the effectiveness of Kohn-Sham DFT.

The exchange-correlation (XC) functional contains all contributions to the electronic energy that are not included in the other three terms.[50] Dynamic correlation refers to the motion of electrons caused by instantaneous Coulombic interactions with other electrons, static correlation is the reduction in total energy caused by multiple possible electron configurations, and exchange refers to the non-Coulomb repulsion due to the Pauli exclusion principle. This functional also includes some corrections including one for the approximate nature of the non-interacting orbitals used for the kinetic energy and another for the interaction of each electron with itself. The true form of this functional is unknown, but approximations exist, generally based either on the physics of electron-electron interactions or on fits to experimental data.[51] While the first solution seems more conceptually elegant, the second often yields greater accuracy.

The most basic version of the XC functional is referred to as the local density approximation (LDA) and is based purely on the electron density.[52] This is not a very good approximation for molecules and does not produce accurate results for molecular properties. Allowing the functional to depend on the gradient of the density as well as its magnitude yields significant improvement in accuracy, a modification called general gradient approximation (GGA). GGA XC functionals are quite popular. To improve on the GGA method, some Hartree-Fock energy can be included in the XC functional. This forms the basis of hybrid functionals.[53] From GGA and hybrid functional methods, further improvements can be obtained by incorporating higher-order derivatives of the electron density, but this is very computationally intensive so the majority of DFT calculations are performed using GGA or hybrid functionals.

Using such methods, DFT can be used to obtain a high level of accuracy at quite low computational expense, and these superior models of XC functional are a key reason for the popularity of DFT in modern quantum chemistry calculations. In this thesis, all calculations were performed using a hybrid functional called B3LYP.[53, 54]

IV. Basis Sets

The artificial wavefunctions used in Kohn-Sham DFT are represented as a set of Kohn-Sham molecular orbitals which are each a linear combination of basis functions, $\chi(\mathbf{r})$:

$$\psi_i(\mathbf{r}) = \sum_{\nu=1}^{K} c_{\nu i}\chi_\nu(\mathbf{r}) \tag{8}$$

Here ν is the index of the basis functions, K is the total number of basis functions and $c_{\nu i}$ is a coefficient representing the contribution of each basis function to the molecular orbital. It is these coefficients that are adjusted when optimizing the wavefunction to minimize the electronic energy. The basis functions themselves remain unchanged. The various forms of basis functions will be discussed in this section. Basis functions can take any mathematical form, but there are certain forms which are more popular than others. This section will focus on atom-centered functions, particularly Pople basis functions, as this is the type of basis function employed in obtaining the results presented in this thesis.

Atom-centered or localized basis sets work on the assumption that a molecular wavefunction is a combination of atomic orbitals, which are centered on the nuclei of the atoms in the system. The well-known hydrogen atom solution to the Schrödinger equation indicates that orbitals decay exponentially with increasing distance from the nucleus and are directionally dependent on the angular momentum of the system. Slater functions fit this behaviour well:

$$f_S(\mathbf{r}) = Nx^a y^b z^c e^{-\alpha|\mathbf{r}-\mathbf{R}|} \tag{9}$$

In this type of function, N is a normalization constant, a, b and c are non-negative integers and α is a parameter. The $x^a y^b z^c$ part of the function is the angular part, and allows this type of function to describe orbitals well. The sum of the integers a, b and c is equal to l, the angular momentum quantum number for the orbital. Thus, for s-orbitals where l=0, there is no angular part of the orbital, and for p-orbitals a, b or c will be equal to 1 while the others are zero, leading to a set of three orbitals each aligned along a different spatial coordinate. The exponential part of the function is the radial part, and controls how fast the orbital decays when moving away from the nucleus, which is at **R**. Thus, a Slater function is centered on a nucleus, is directionally dependent on angular momentum and decays exponentially with distance from the nucleus, which are the constraints required for a localized basis function. Slater functions make excellent atomic orbitals for quantum chemical calculations in terms of accuracy, but there are calculations which must be performed in solving the Schrödinger equation which cannot be analytically determined using these functions. Thus, using Slater functions directly as atomic orbitals is quite computationally difficult.

An acceptable solution which sees a great deal of use in quantum chemistry is the adoption of Gaussian functions instead of Slaters. A Gaussian function is similar to a Slater function, except that the decay of the function is based on the square of the distance from the nucleus, as seen in equation 8. All variables in the Gaussian expression are defined the same as those in the Slater expression, although the normalization constant has a different form. A comparison of the shapes of these two functions can be seen in Figure 2.4. It can be seen that the Gaussian lacks a cusp at the nucleus and decays too quickly at high r, but still shows much similarity to the Slater function.

$$f_{\mathrm{G}}(\mathbf{r}) = Nx^a y^b z^c e^{\alpha|\mathbf{r}-\mathbf{R}|^2} \tag{10}$$

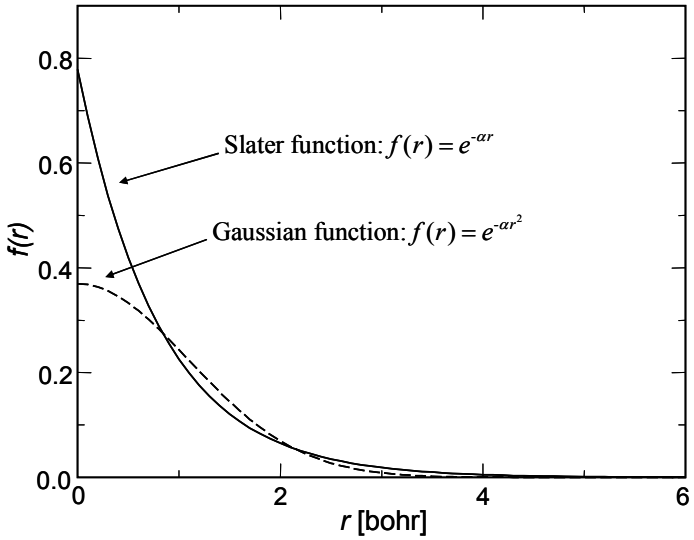

Figure 2.4: A comparison of the shapes of the radial components of Gaussian- and Slater-type functions. It can be seen that Gaussian functions decay too slowly near the nucleus and too quickly at large distances, but the overall shapes of the functions are similar. The angular parts of these two functions are identical.

Improvements on the basic features of a Gaussian function can be obtained with "contracted" Gaussian functions constructed from a linear combination of "primitive" Gaussians. By doing this, a number of different decay constants can be incorporated into the function, which adjusts the decay rate to improve the quality of the Gaussian as compared to the Slater, but without introducing the calculation difficulties inherent with using Slater functions. Figure 2.5 compares a Slater function to a number of contracted Gaussians and it can be seen that the shape of the contracted Gaussian is much improved.

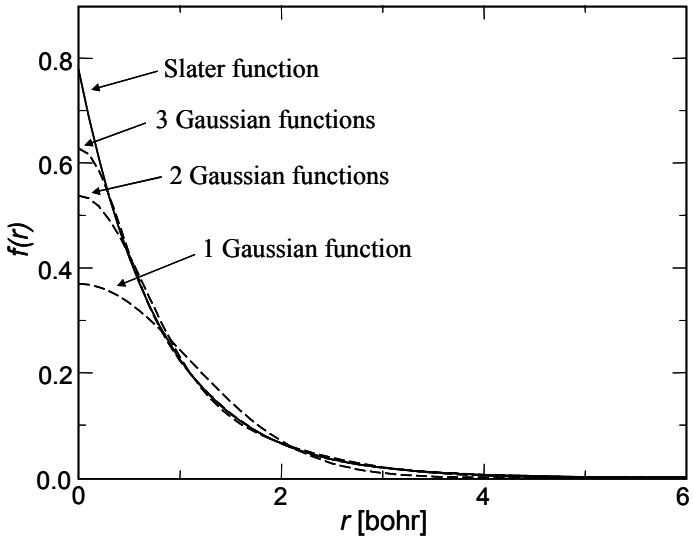

Figure 2.5: A comparison of a Slater function to contracted Gaussian functions made up of 1, 2 or 3 primitive Gaussians. It can be seen that the more Gaussians are used, the closer the two functions become, to the point where a contracted function of 3 Gaussians closely resembles the Slater function, although it still lacks the cusp at the nucleus.

Basis sets constructed from contracted Gaussians are the most popular form of atom-centered basis functions used in DFT. In general, multiple basis functions are used for each atom in a system, and this is referred to as a basis set. The basis sets employed in the current work are all of the Pople form.[55] Each Pople basis set has a label of the form X-YG. In a basis set of this type, core and valence electrons are described with different sets of basis functions. X denotes the type of functions employed in the core, while Y describes the valence functions. G indicates that the basis functions are all Gaussian in form. For example, the very popular 6-31G basis set utilizes contracted functions of 6 primitive Gaussians for the core electrons of an atom, while valence electrons are described using two different basis functions, one of which is a single Gaussian function and the other is a contracted Gaussian function built from 3 primitives. The number of digits in each term is referred to as "zeta", hence 6-31G is a valence double-zeta basis set which uses two basis functions for each valence electron. A slightly improved basis set is 6-311G, which is a valence triple-zeta basis set. Single-zeta sets are rarely used as their accuracy is quite low and only suitable for rapid qualitative calculations.

Two other common features of Pople basis sets bear explanation at this point; these are diffuse and polarization functions, denoted "+" and "*". 6-31G** is one of the most popular Pople basis sets and is the one employed in our research. The presence of the asterisk indicates the use of polarization functions. The presence of two asterisks indicates that they will be used on all atoms, whereas one asterisk would leave these functions off of hydrogen and helium atoms. Polarization functions take the form of higher angular-momentum functions than those that would normally be employed. On an atom such as carbon, which normally has s and p type orbitals, the polarization functions used would have the form of d-type orbitals. 6-31++G would be a basis set employing diffuse functions. These functions decay very slowly and are used in calculations involving hydrogen bonds, anions or excited states. A very accurate Pople basis function might have the form 6-311++G**, employing a triple-zeta basis set with diffuse and polarization functions on all atoms, but in many cases this is much more accurate than necessary for the associated computational cost, and it is necessary to determine on a case-by-case basis whether higher zeta, diffuse or polarization functions are necessary for a given system.

Atom-centered basis functions are very popular in quantum chemistry because they can produce accurate results with a relatively small number of basis functions. Gaussian functions are much more convenient to use than Slater functions, though it can be quite difficult to approach high levels of accuracy with contracted Gaussians; a great many functions could be needed. There are drawbacks to this kind of basis function, based on the fact that the functions are atom-centered. Such a function does not treat all parts of space equally which causes problems when calculating properties such as reaction energies for processes such as dissociations. These errors tend to be small, but are worth noting.

V. Geometry Optimizations

In quantum chemistry one of the most common goals is to identify the structures of key species in chemical reactions and their accompanying energies. These species include reactant, products, transition states and intermediates. The common feature of all these is that the first derivatives of the potential energy surface (PES) with respect to the nuclear coordinates at these locations is zero. Since the first derivative corresponds to the forces acting on the system, these points where the forces are zero are termed stationary points. Searching the PES for these stationary points is a very common type of quantum chemical calculation, and the calculations performed for this thesis were all of this type.

Reactants, products and intermediates along reaction pathways correspond to minima on the PES. A minimum is defined as a point where all first derivatives of the energy with respect to atomic positions are zero as described above and all second derivatives are positive. Many minima can be found on a potential energy surface, and for a reactive system these will include the reactants, products and any intermediates, as well as additional minima which do not lie along the reaction coordinate of interest. The lowest-energy minimum on the PES is termed the global minimum while all others are local minima. Transition states on the other hand occur at locations called first-order saddle points, where all first derivatives are zero and all second derivatives are positive except for exactly one, where the second derivative is negative. The direction in which the negative second derivative is found corresponds to the reaction coordinate. There are many first-order saddle points found on a PES, but they do not all correspond to relevant transition states. The method of identifying which saddle point corresponds to the transition state will be described below.

Locating the minima and transition states on the PES requires finding points which satisfy the criteria described above, but a comprehensive search is not feasible due to the 3N-6 dimensionality of a PES, where N is the number of atoms in the system. Optimizing to a minimum or transition state geometry requires some kind of guided method. These methods generally use the first and second derivatives of the energy with respect to nuclear positions. The first derivatives are easily obtained by quantum chemical methods but the second derivatives are much more difficult and are usually estimated. An initial guess for the geometry at a minimum is used as a starting point, and calculating the electronic energy of this system provides the forces on the nuclei (first derivatives) and an estimate of the curvature of the PES (second derivatives). Using this, the geometry is altered in such a way that the forces should be reduced until a certain cutoff is reached at which point the forces are assumed to be close enough to zero. At this point, the system is deemed to be at a stationary point, but characterizing the type of stationary point requires further calculations to determine the second derivatives accurately. This is done using frequency calculations. It should be noted that the entire process outlined here can be extended to the force-modified system used in this thesis, as the first and second derivatives of *Fx* are straightforward to obtain and can be added to the corresponding quantities from the Born-Oppenheimer PES.

VI. Frequency Calculations

Vibrational frequencies are of great importance in studying molecules via quantum chemistry. Calculating these frequencies can allow for the estimation of vibrational spectra, zero-point energies and thermodynamic energy corrections. They can also be used to characterize stationary points on the PES. The harmonic approximation is used to calculate

vibrational frequencies, and this is most valid at stationary points where the forces on the nuclei are zero. For instance, the bond of a diatomic molecule can be approximated as a one dimensional harmonic oscillator, as shown in equation 11.

$$E_{vib}^{n} = h\upsilon(n + 0.5) \tag{11}$$

In this equation, h is Planck's constant, n is the quantum number of the vibrational state and v is the vibrational frequency, as given in 8.

$$\upsilon = \frac{1}{2\pi}\sqrt{\frac{k}{\mu}} \tag{12}$$

Here, k is the force constant for the bond and μ is the reduced mass of the system. And finally, the force constant k is given by equation 13:

$$k = \frac{\partial^2 V}{\partial R^2} \tag{13}$$

Thus, the force constant is calculated from the second derivative of the electronic energy, V, with respect to the length of the bond, R. Using equations 11 through 13 it can be seen that the energy and frequency of a vibrational mode are related to the square root of the second derivative of the energy with respect to the nuclear coordinates, which was described above as being important for characterizing stationary points on the PES but difficult to calculate directly from the electronic energy of the system.

Using vibrational frequencies allows for the characterization of stationary points without requiring precise knowledge of the curvature of the PES. At a minimum on the surface, the curvature should be positive in all directions, and since we know this is related to the square of the vibrational frequency, we know that all the vibrational frequencies should be real, positive integers since the square root of a real number is another real number. On the contrary, at a transition state there should be exactly one direction which has a negative curvature. Since the

square root of a negative number is an imaginary number, this means that exactly one vibrational mode of a transition state should have an imaginary frequency. Thus, if a stationary point has all real vibrational modes it represents a minimum on the PES, while one with one imaginary mode represents a transition state. Since the imaginary mode represents the reaction coordinate, it is also possible to follow this mode to discern whether the transition state is actually located between reactants and products along the reaction coordinate.

VII. Kinetic Models

In this thesis, we seek to investigate whether mechanochemistry can be developed into a synthetically-useful method of lowering reaction barriers. This barrier reduction leads to an increase in the rate of reaction and thus an increase in the amount of product obtained in a given time period. In order to understand and quantify this effect, a discussion of the relationship between reaction barriers and reaction rates, and how these are affected by mechanochemistry, is required. To begin describing the rates of mechanically-modified reactions, it must be noted that chemical reactions proceed via a mechanism that converts some reactant molecules to products by way of a transition state. This process follows a reaction coordinate along a potential energy curve containing an energetic barrier. In the case of a mechanochemical process, this is made more interesting by the fact that the mechanical force is seen to perturb the shape of the potential energy surface. This can be seen in Figure 2.6.

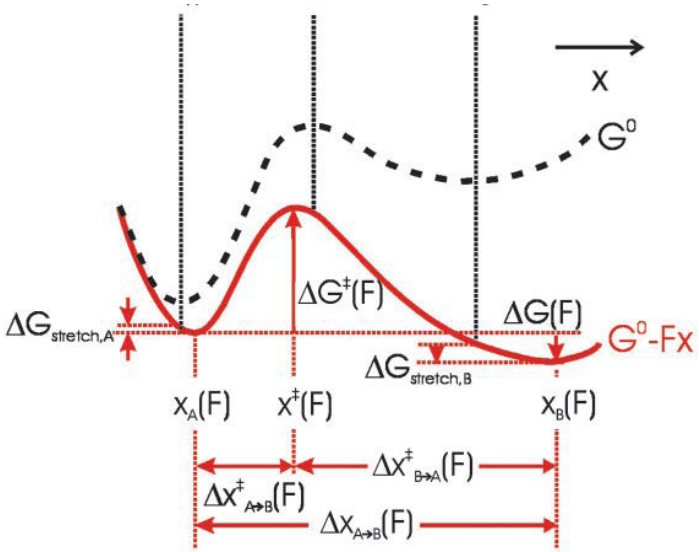

Figure 2.6: The effects of an applied force on the free energy curve for a reaction. Similar behaviour is seen in potential energy surfaces like those described in this thesis. The dotted line indicates the curve without applied force, and the solid red line is the curve with an applied force. This force lowers the energy at reactants, products and transition states, but to differing amounts. Large reductions in transition state and product energies lead to lower reaction barriers, faster reaction rates and larger product yields. The locations of both minima and the maximum also change under applied force.[26]

A reaction like this can be described very simply as R → P, where R represents reactants and P represents products, and the rate of such a reaction is generally described by

$$\frac{d[P]}{dt} = k[R]^{r\prime} \tag{14}$$

Here, the rate of the reaction is represented by the rate of the formation of products, which is proportional to the concentration of the reactants, $[R]$, to an exponent based on their stoichiometry, *r'*. If multiple reactant species are present, each will have its own exponent. The proportionality constant, *k*, is referred to as a rate constant. The most common expression used to determine the rate constant for a reaction is the Arrhenius equation, which is an empirically-derived equation.

$$k = Ae^{-E_a/RT} \tag{15}$$

Here, A is an empirically-determined factor known as the Arrhenius pre-exponential factor, R is the ideal gas constant, T is the temperature and E_a is the activation energy. The Arrhenius equation is generally accurate for calculating the temperature dependence of a reaction rate, since T is the only non-constant in the equation, but it has significant failings in that the activation energy and pre-exponential factor are both empirical quantities, and so this equation cannot be used to estimate the rate of a reaction without performing experiments or calculations.

A modified version of the Arrhenius equation was suggested by Zhurkov to describe the mechanical degradation of polymers.[56, 57] In this equation, work done by the grinding or milling process modifies the activation energy for the reaction:

$$K = K_0 e^{-(E_A - W)/RT} \tag{16}$$

Here, W represents the work done by the stress of milling. This rate equation is related to Bell's model,[58] which describes the reaction barrier of a stretched system as:

$$E^{\ddagger} = E_0^{\ddagger} - F\Delta x_0 \tag{17}$$

Here, $E_0^{\ddagger}$ represents the reaction barrier without applied force, and Δx_0 is the change in distance between pulling points in going from reactants to products, both without applied force. F is the magnitude of the applied force. So long as extension is carried out slowly enough to keep the system in quasi-static equilibrium, the work induced by this force is reversible and represents a change in the energy of the system. Thus, the total reaction barrier described here is analogous to the numerator of the exponential in equation 14. In this treatment, only the force changes so

any change in rate or energy is attributed to the work term. This is incorrect, as the application of force induces changes in geometry which change the shape of the potential energy surface for the reaction, as seen in Figure 2.6. This will be explored further later on.

The modified Arrhenius equation described above is unable to accurately predict changes in rates for mechanically-modified reactions. As such, more advanced kinetic models based on Transition State Theory (TST) should be used. Though kinetic studies were not performed as part of the body of results presented here, an overview of TST follows, as this method would be appropriate for describing the systems under study, and supports the results obtained and conclusions drawn.[59]

TST makes some very important assumptions: notably, that a transition state exists at the highest energy point on a reaction coordinate and that this transition state can be used to determine the rate of the reaction, and that this transition state is in quasi-equilibrium with the reactants. The equilibrium constant for this equilibrium is denoted $K^{\ddagger}$, and is given by:

$$K^{\ddagger} = \frac{[TS]}{[R]} \tag{18}$$

$[TS]$ represents the concentration of transition state molecules, and $[R]$ the concentration of the reactant. Using $k^{\ddagger}$ as the rate constant for the conversion from transition state to products, the rate of the overall reaction is given as follows:

$$\frac{d[P]}{dt} = k^{\ddagger}[TS] = k^{\ddagger}K^{\ddagger}[R] = k[R] \tag{19}$$

Making use of the following definition of Gibbs free energy,

$$\Delta G = -RTlnK \tag{20}$$

We can write the equilibrium constant as

$$K^{\ddagger} = e^{-\Delta G^{\ddagger}/RT} \tag{21}$$

Also, it should be noted that the rate constant $k^{\ddagger}$ is associated with one of the vibrational modes in the transition state. The forward rate of the reaction through the transition state cannot be faster than the frequency of the vibrational mode corresponding to the transition state. This leads to the temperature dependence given in equation 22:

$$k^{\ddagger} = \frac{k_b T}{h} \tag{22}$$

where h is Planck's constant. Thus, the rate constant for the overall reaction is given by:

$$k = \frac{k_b T}{h} e^{-\Delta G^{\ddagger}/RT} \tag{23}$$

The relevance of this equation to the work presented herein is as follows: if temperature is taken to be a constant, the only variable in this equation is the change in Gibbs free energy obtained in going from reactants to transition state. Due to this, we can predict that a decrease in the energy barrier will result in a decrease in the magnitude of the exponential term, thereby leading to an overall increase in the rate constant and thereby the reaction rate. Also, unlike models such as Bell's Model or the modified Arrhenius equation proposed by Zhurkov, this model does not explicitly include a work term, instead incorporating any mechanical modification into the PES for the reaction. This allows for any change in the total barrier, mechanical or otherwise, to induce a corresponding change in reaction rate. In this thesis, reaction barriers are expressed in potential energy rather than Gibbs free energy, but it can be safely assumed that the trends will be very similar. This is due to the fact that Gibbs free energy incorporates both entropy and enthalpy of reactions; enthalpy changes should mirror the potential energy changes described in this thesis, and entropy changes for the systems we studied should not have a profound effect on the barrier changes obtained. This similarity in trends allows for the prediction that a decrease in potential energy barrier will still correspond to an increase in rate.

Chapter 3: Results

I. Overview

It is intuitive that a unimolecular reaction involving bond-rupture should be accelerated by the application of a force across the scissile bond. Such processes have been studied extensively using both experimental and theoretical methods. [11, 14-19, 21, 22, 31, 32, 34-36, 38] A less-studied area involves the mechanochemical activation of reactions involving more than one molecule and/or where there is no scissile bond. Given the extensive use of such reactions in chemical applications, the investigation of the mechanochemical activation of these processes offers an exciting avenue for our research. In this Chapter we report the results of theoretical studies into the mechanochemical control of bimolecular reactions involving additions to alkenes. Two different reactions are considered. The first reaction involves the hydration of 2-butene. This reaction was investigated to explore the possibility of using mechanical stress to render a C-C single bond more reactive than a neighbouring C-C double bond. The second reaction involves the addition of nitrones to the C-C double bond in various alkene substrates. This reaction does not involve the cleavage of any bonds, and thus is a departure from conventional mechanochemical studies, which focus on reactions involving the rupture of bonds. The results demonstrate that mechanical stress can be used to affect the outcomes of bimolecular reactions. This occurs in two ways. First, the application of mechanical stress performs work on the system that effectively reduces the barrier as discussed in Chapter 1. Second, the application of stress deforms the molecule, which can alter intermolecular interactions, especially sterics, in a manner that alters the reaction barriers. Means of controlling the application of mechanical stress to take full advantage of these effects are also examined. Overall, this work represents one of the first theoretical investigations of the mechanochemical activation of bimolecular reactions,

demonstrates that mechanical stresses can indeed be used to control these reactions, sheds light on the origin of these effects, and provides insight regarding the rational design of molecular systems that can be activated through applied mechanical stresses.

The remainder of this chapter is as follows. Section II provides a brief overview of the methods that were used to perform the calculations. The hydration of 2-butene is discussed in Section III. The addition of nitrones to straight-chain alkenes is discussed in Section IV, the addition to alkenes in rings in Section V, and the addition to alkenes in substituted rings is discussed in Section VI. The contributions of the mechanical work and changes in the Born-Oppenheimer potential energies of the reactants and transition states to the changes in the barriers are discussed in Section VII.

II. Methods

All calculations described in this section were performed with the NWCHEM software package, which was modified in order to perform calculations according to the EFEI formalism.[37] The Born-Oppenheimer contributions to the EFEI energy were obtained using density functional theory calculations with the B3LYP exchange-correlation functional[53, 54] and the 6-31G(d,p) basis set described in Chapter 2. This method has been used previously to study the addition of nitrones to alkenes, with results demonstrating that it yields reaction barriers within 2-3 kcal/mol of those obtained from CCSD(T) calculations.[60] Larger basis sets were also tested. Moving to a valence triple-zeta basis set yielded barriers approximately 3 kcal/mol higher than those obtained with the valence double-zeta set. The reactant and transition state structures were optimized directly on the force-modified potential energy surface. Frequency calculations were performed to ensure that all minima exhibited normal modes with only real,

positive frequencies, and all transition states exhibited exactly one normal mode with an imaginary frequency.

Caution must be employed when using DFT methods to investigate bonds that are being stretched by applied mechanical stress. Specifically, as the bonds are elongated, they will start to dissociate and adopt diradical character. It is well-known that DFT methods are not formally capable of describing diradical structures, although they often work well in practice, which may be a cause for concern. Analysis of how the bond lengths change with applied forces indicates that the adoption of diradical character is not a concern for the force ranges considered in this work. As an example, consider Figure 2.2, which shows that the equilibrium bond length of a C-C bond represented by a Morse potential elongates by only 0.1 Å with an applied force of 3000 pN. The systems reported below also exhibited only minor changes in equilibrium bond lengths, with angles and torsions being more significantly altered by the applied force. As such, we are confident in the ability of DFT calculations to properly describe the systems discussed below.

III. Hydration of Carbon-Carbon Double and Single Bonds

The application of mechanical stress will most significantly affect weak degrees of freedom. On this basis, one can anticipate that single bonds in molecules will be more sensitive to applied stress than double bonds, which are stiffer. This difference in the expected responses of different bonds to applied stresses leads to the possibility of using mechanical stresses to render single bonds more reactive than double bonds. If achieved, this 'reactivity switching' would have significant synthetic potential because C-C double bonds are nearly always more reactive than C-C single bonds, yet there may be cases where activating single bonds would be

advantageous. To explore this possibility, we identified several textbook reactions involving the addition of various species to carbon-carbon double bonds. We then considered the analogous reaction involving the addition of the same species to a C-C single bond in the same molecule. The reaction that was the focus of our attention involved the concerted addition of water to 2-butene, which is shown in Figure 3.1. The addition at the double bond involves the dissociation of an O-H bond in water to add a hydrogen atom to one carbon in the C-C double bond and an OH group to the other, yielding 2-butanol. The single-bond hydration we studied involved cleaving one of the C-C single bonds in 2-butene, adding an OH group to one end of the C-C double bond and a hydrogen atom to the methyl group, yielding methane and 1-propenol.

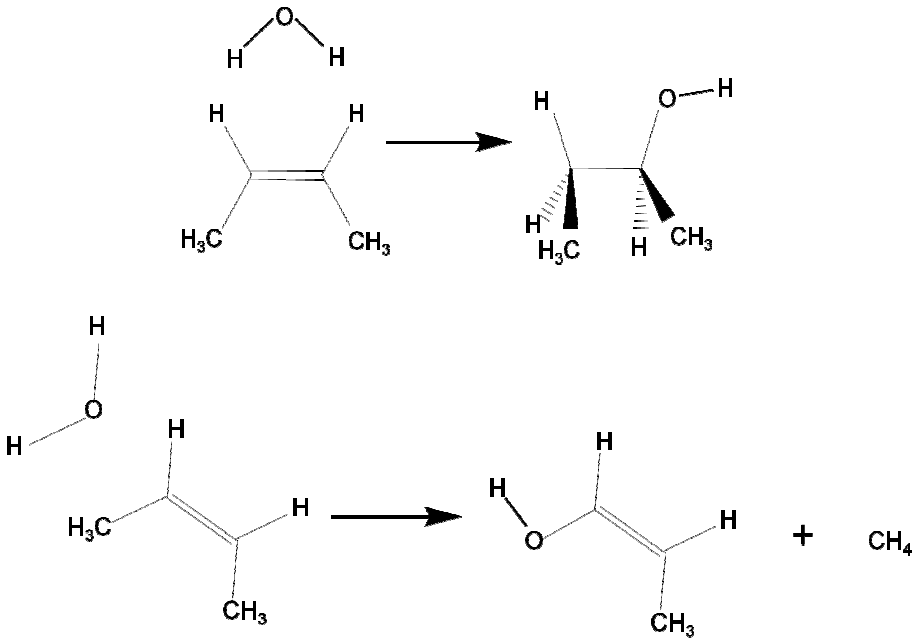

Figure 3.1: Hydration of 2-butene at the C-C single and double bonds.

Transition states were located for the hydration of the C-C double bond in 2-butene and for the hydration of an adjacent C-C single bond. The transition state structures calculated with F=0 pN are shown in Figure 3.2. Barriers were calculated for both reactions as a function of applied force. These results are shown in Figure 3.3. The data in Figure 3.3 show that the

hydration of the double bond is accelerated by applied force, with the barrier decreasing from 47.5 kcal/mol to 29.5 kcal/mol over a range of F=0 to 6000 pN, representing an increase in rate constant of approximately 18 orders of magnitude. The data for the addition to the single bond exhibit a reduction in the barrier, with the barrier decreasing from 101 to 99 kcal/mol over a range of F=0 to 1000 pN. Despite the magnitude of this change lying within the energy uncertainty of a DFT calculation, the trend represents a difference of differences of energies and should have relatively low uncertainty. Unfortunately, the transition state for this reaction was unable to sustain forces greater than 1200 pN, and thus it is not possible to evaluate the barriers at higher values of F_{ext}.

Analysis of the data shows that the barrier versus force curve for addition of water to the single bond has a steeper slope than that for the addition to the double bond. This suggests that the hypothesized reactivity switching may be possible if the transition state for addition to the single bond could sustain higher forces. Fitting the two curves to quadratic functions, as suggested by a model developed within the Mosey group, suggests that the two curves should intersect when F=3000 pN. Overall these results suggest that reactivity switching may be possible in other cases if the system can withstand the high forces needed to achieve the switch in the preferred reactive site. The possibility of switching may also be increased in reactions where the difference in the barriers for addition at the single and double bonds is lower when F=0 pN, implying that lower force-induced changes in the barriers would be needed to achieve the switching effect. We were unable to find other reactions involving the addition to alkenes that seemed to offer this potential, and thus this line of research was stopped. However, the possibility of achieving stress-induced reactivity switching in other systems may be an interesting avenue for further research.

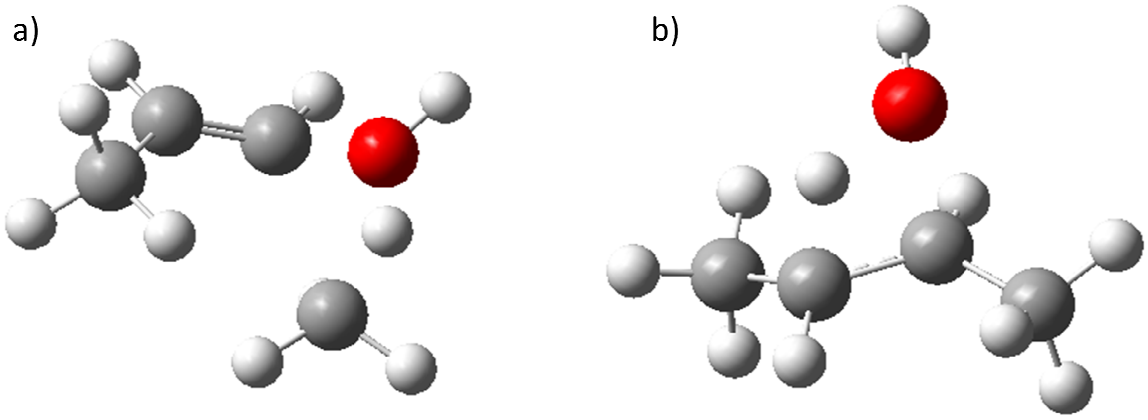

Figure 3.2: Transition state geometries for hydration reactions to butene. Image a) shows the hydration to the double bond in butene, which is the normal reaction, though it is usually acid-catalyzed. Image b) shows the hydration to the single bond. Note that the bond is already stretched in this structure to a point where the imaging software does not draw it.

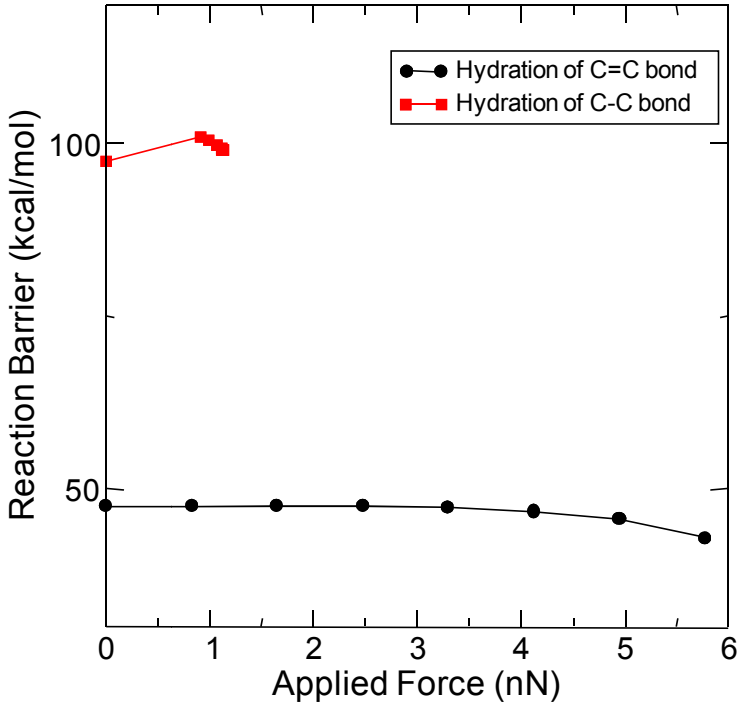

Figure 3.3: Barrier vs force curves for hydration reactions. A steady decrease in the barrier as a function of applied force is seen for the hydration of the carbon-carbon double bond in butene, while a significantly steeper curve is seen for hydration of the single bond. The single bond transition state is unfortunately unable to support forces above 1200 pN, so curve crossing is not observed, but the trend seems to indicate it would otherwise be possible. However, even if this were the case, the absolute reaction barriers are far too high to be experimentally accessible.

IV. Force-Modified 1,3-Dipolar Cycloaddition of N-Methyl Nitrone to Alkenes

The study of the hydration of alkenes discussed in Section III indicates that the barriers to bimolecular reactions can be affected through the application of external force. The results in that section also demonstrated that it is important to ensure that these effects can be achieved within force ranges that can be supported by the system under investigation. Combined, these observations motivate us to explore other bimolecular reactions that do not involve bond scission under conditions of relatively low applied stresses. For this purpose, we will investigate the 1,3-dipolar cycloaddition of N-methyl nitrone (Figure 3.4) to alkenes, which is also referred to as a Huisgen reaction. This reaction occurs through the concerted formation of a C-C and C-O bond, as shown in Figure 3.4, and is used in the synthesis of isoxazolidines, which are important heterocyclic rings found in such species as HIV drugs,[61] antifungal agents,[62] and synthetic oligopeptides.[63] As such, understanding the effects of mechanochemistry on this reaction is of direct application in organic synthesis. The reaction is also appealing from the standpoint of the calculations performed in the present study because the mechanism is known and has been explored in detail in previous studies,[60,64] which provides us with information regarding the structures of the reactants, products and transition state.

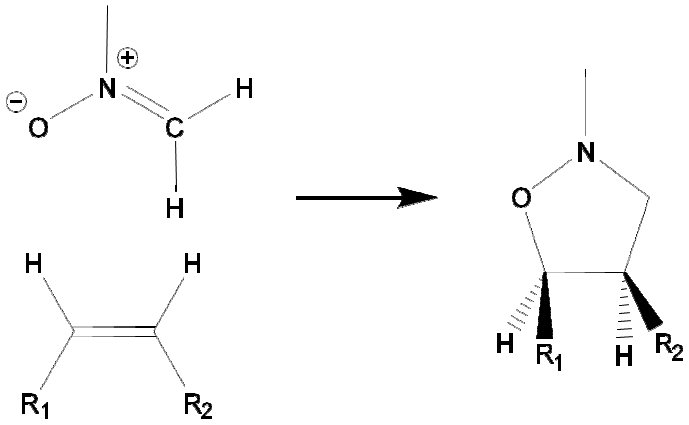

Figure 3.4: The concerted formation of a C-C and C-O single bonds by the Huisgen reaction. Also during this reaction, C-C and C-N double bonds are reduced to single bonds and in the process several carbons undergo changes in hybridization.

a. Structures and Behaviour when F = 0 pN

In the present study, the nitrone moiety for the reaction was kept constant as N-methyl nitrone, while the alkene moiety was varied. The specific alkenes considered in the calculations were ethene, 2-butene, 3-hexene, 4-octene, 5-decene and 3,3,6,6-tetramethylcyclohexene (TMCH). A summary of the barriers and key geometric details obtained with $F = 0$ pN are given in Table 2 and can be used as a reference point when considering the effects of applied forces on the barriers and geometries of these systems. Knowledge of the barriers in the absence of an external force is necessary to gauge the effects of the applied stress on the barriers to the reaction. Meanwhile, knowledge of how the degrees of freedom (DOF) change upon progressing from the reactants to the transition state is of value in terms of rationalizing the effects of the applied stress. Specifically, the EFEI model suggests that the barrier to a reaction will decrease if the force is applied between pulling points (PPs) that naturally separate as the system moves from the reactant to the transition state because Δx in Eq. 2 of Chapter 2 will be positive. As such, understanding how the DOFs naturally change, and how this change is affected by the applied stress, can be useful in interpreting mechanochemical effects.

Table 2: Reaction barriers for each of the Huisgen reactions simulated in this study, along with those geometric degrees of freedom closest to the scissile bond in this reaction, in both reactant and transition state.

Alkene Substrate	D_{12} (Å)	θ_{123} (○)	φ_{1234} (○)	Barrier (Kcal/mol)
Ethene (r)	1.330	N/A	N/A	11.6
Ethene (ts)	1.382	N/A	N/A	11.6
Butene (r)	1.335	125.3	N/A	15.8
Butene (ts)	1.500	123.0	N/A	15.8
Hexene (r)	1.335	125.5	119.2	16.9
Hexene (ts)	1.390	122.9	-169.7	16.9
TMCH (r)	1.336	125.2	133.2	23.0
TMCH (ts)	1.401	122.5	144.0	23.0

The reactant and transition state geometries for the addition of N-methyl nitrone to hexene are shown in Figure 3.5. The changes in DOFs in this reaction when going from reactant to transition state are fairly straightforward, but can shed light on changes in the geometry that may be related to mechanochemical activation. Throughout the overall course of the reaction, the C-C double bond is converted to a single bond, and the carbon centers in the C-C double bond undergo a change from sp^2 to sp^3 hybridization. The transition state exhibits a structure between these two extremes. Specifically, D_{12} bond stretches from 1.34 to 1.39 Å as the system moves from the reactant to the transition state, while θ_{123} angles decreases from 125.5° to 122.9°. In the case of φ_{1234}, the magnitude of the deformation is difficult to quantify, but it is observed that the torsional angle approaches 180°, which is known to be the high-force limit for this DOF. Similar trends are exhibited by the other substrates considered, except in the cases of ethene and 2-butene which do not contain all these DOFs. Overall, this analysis of the structural changes indicates that applying an external force in a manner that increases D_{12}, decreases θ_{123} and flattens φ_{1234} towards 180° will lead to a decrease in the barrier. An increase in the barrier is

expected if the applied force has the opposite effect on the DOFs. Of course, it is possible for the applied force to alter some DOFs in a manner consistent with progression of the reaction and other DOFs in a manner that counters the reaction's progress. The specific effects of applied forces on the geometries of the systems and the associated barriers are discussed in the following sections.

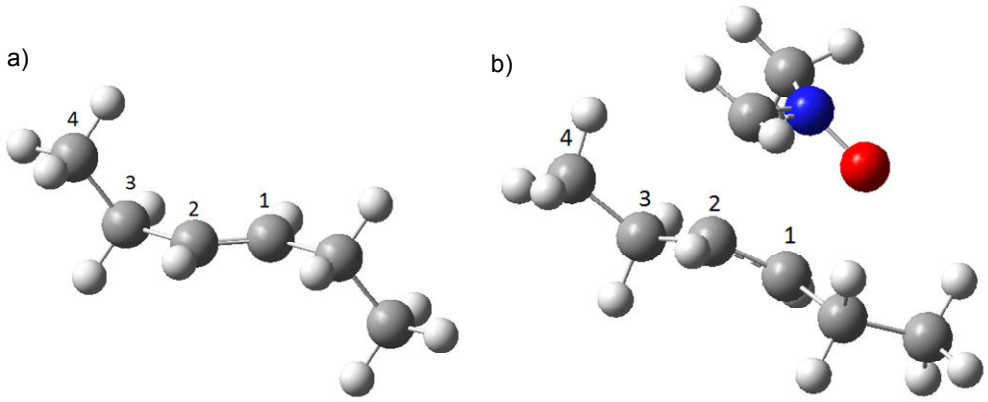

Figure 3.5: a) the reactant structure of the 3-hexene substrate and b) the transition state for this substrate undergoing a Huisgen reaction with N-methyl nitrone. The numbering given in this Figure is used throughout this study, where 1 and 2 denote the carbons in the reactive bond, and 3 and 4 are used to describe geometric degrees of freedom involving this bond, ie the 1-2-3 bond angle and the 1-2-3-4 torsional angle. From this Figure it can be observed that many degrees of freedom have been deformed in going from reactant to transition state, and it is theorized that if these degrees of freedom are similarly deformed under mechanical force, a reduction in reaction barrier will be seen.

b. Behaviour with Straight-Chain Substrates when F > 0 pN

The first substrates considered for the addition of nitrones to alkenes under mechanochemical conditions consisted of straight-chain molecules with the C-C double bond in the centre. Five different alkenes were considered in these calculations: ethene, 2-butene, 3-hexene, 4-octene and 5-decene. For all five systems, the terminal carbon atoms were used as pulling points.

Figure 3.6 shows the changes in the reaction barriers with increasing *F* for each system. The curves obtained from calculations with the ethene and butene substrates are quite different from those obtained with hexene, which yields results similar to those obtained when pulling on octene and decene. This can be attributed to the different DOFs affected by the applied force. When pulling from the terminal carbons of ethene, the only DOF being affected is the carbon-carbon double bond. In a reaction such as this, where the C-C double bond undergoes a decrease in bond order to form a single bond and increases in length by 0.05 Å upon progressing from reactants to transition state, stretching this bond decreases the reaction barrier. However, the reduction in the barrier is only 1 kcal/mol at $F = 0$ pN because the carbon-carbon double bond has a very high force constant, calculated to be 946 N/m, and thus requires the application of large forces to lengthen significantly. Using this force constant and assuming harmonic behaviour, it would require 4.7 nN to stretch the carbon-carbon bond in ethene to its transition state length.

Pulling from the terminal carbons of butene, the affected degrees of freedom include the C-C double bond, the two carbon-carbon single bonds, and the two C-C-C bond angles. It is generally easier to deform angles than it is to stretch bonds, so the angles are more significantly affected by the applied force. As described above, as this reaction progresses from reactant to transition state the bond angles should decrease from 125.5 to 122.8°. When stretching 2-butene, these angles are increased instead, reaching 129.2° when F=2000 pN. This counters the natural change in these angles during the reaction, increasing the reaction barrier as seen in Figure 3.6.

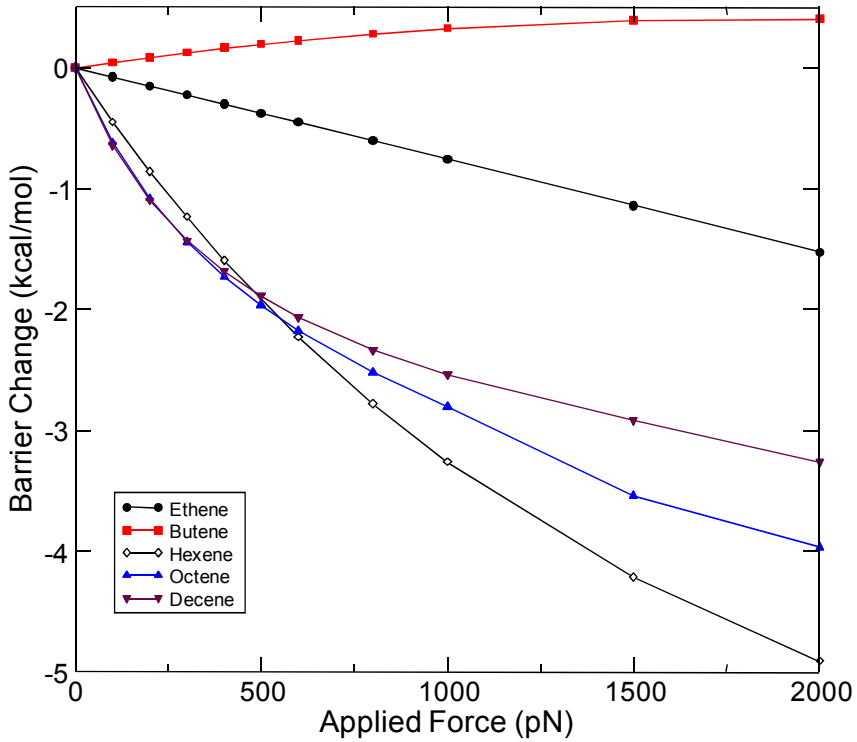

Figure 3.6: Barrier change as a function of applied force for N-methyl nitrone cycloaddition to five different straight-chain alkene substrates. It should be noted that ethene and butene show distinctive curves, while all chains with six or more carbons are similar in shape and magnitude.

The change in barrier versus *F* plots obtained with hexene, octene and decene are all similar to each other and distinctly different than those obtained with ethene and butene. Once again, this can be understood in terms of the DOFs that are affected by the applied force. Specifically, when employing hexene, or longer chains, the affected DOFs include bond lengths, bond angles, and torsions. When describing these DOFs, 1 and 2 are used to denote the carbon atoms in the double bond, as seen in Figure 3.5. Thus, D_{12} is the carbon-carbon double bond distance, while D_{23} is the adjacent single bond, and D_{34} is the single bond adjacent to that. Θ is used to denote bond angles, while φ is used for torsions. Torsions associated with rotation about single bonds are the weakest of these DOFs, and hence most affected by the applied force. This is evident from the data in Figure 3.7, which shows how these DOFs change with applied force. The large torsion effect indicates that simulations involving chains of less than six carbons will

yield very different results from simulations involving chains of hexene or greater, since these longer chains contain single-bond torsions and the smaller ones do not. Since experimental studies of pulling hydrocarbon chains use chains with far more than six carbon atoms,[21, 22, 65] it can be concluded that torsions should be important to any barrier effects. As a result, it appears that any straight-chain substrate with less than six carbons in length is insufficient to simulate this reaction. It is also notable that the barrier changes seen for hexene, octene and decene are very similar in magnitude, supporting the viability of hexene as a model straight-chain for this type of simulations. There is, however, a length dependent effect seen where longer chains show curves which are steeper at low forces and shallower at high forces. This effect has not yet been satisfactorily explained. Work by Marx *et al.*[65] further supports the choice of hexene or longer substrates due to a very large increase in bond rupture force in benzocyclobutene when the polymer handles are extended from one carbon (butene-like) to two carbons (hexene-like). The rupture force changes again in moving to an octene-like system, but the effect is much smaller than the butene-hexene change. The Marx study indicates that for rupture force, chains of at least 12 carbon atoms are required for convergence, but it is intuitive that the effects are smaller when forces are kept well below the bond-rupture regime and thus convergence is approached with a chain of only six atoms.

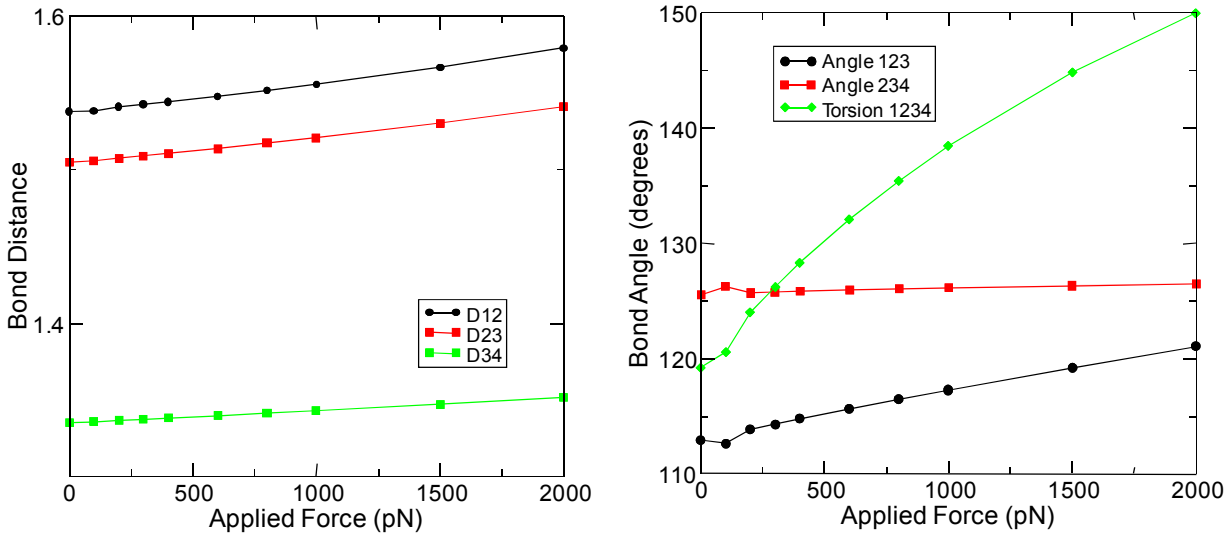

Figure 3.7: Changes in hexene DOFs with increasing force. The change in carbon-carbon single bond length is greater than the change in the double bond length, as expected. The largest overall angle change by far is the 1-2-3-4 torsion. This indicates that torsional effects are significant and should be included in simulations of this reaction.

From studying the effects of force on the addition of N-methyl nitrone to straight-chain alkene substrates, we have observed that reaction barriers do in fact change with *F*, and that the number of carbons in the chain is important to determining what sort of DOFs are affected by *F*. This in turn affects the shape of the barrier versus force curve, wih the curve typical of hexene and longer chains being of the most synthetic relevance. Of large import is that these effects, while noticeable, are fairly small in magnitude. The largest barrier change obtained is for hexene, from 17 kcal/mol to 12 kcal/mol, corresponding to an increase in rate constant on the order of 10^5. Only the largest forces can induce barrier changes which could be synthetically useful. Since current technology makes applying such large forces in a specific manner difficult, other substrates were tried in an attempt to magnify force effects through the chemistry of the reactive system.

V. Nitrone Cycloaddition to Cyclic Alkenes

The results of calculations on straight chain alkenes demonstrate that the ability to reduce barriers through mechanical stresses is limited by the fact that the stresses primarily affect the weakest DOFs. As such, it could be beneficial to design systems in which it is possible to control the weakest DOFs. In the straight-chain systems, the weakest DOFs correspond to torsions. In order to design systems in which these are no longer the weakest DOFs, and instead the applied stress can be directed toward bond lengths and angles, we considered using geometric constraints in the form of rings. The underlying rationale is that a ring contains intrinsic geometric constraints, affecting mostly which torsions are free to rotate. With a stretched ring, the degrees of freedom which are modified will be different from those affected in a stretched straight-chain alkene. By properly inhibiting torsions, it should thus be possible to apply force to the DOFs that are more relevant to the reaction.

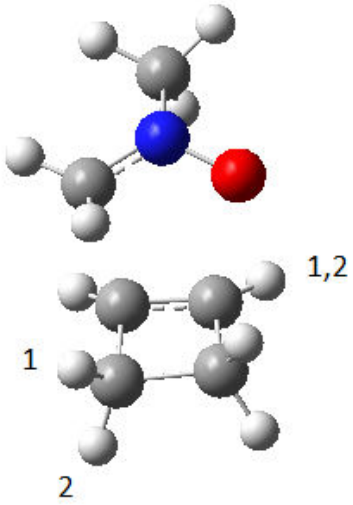

Figure 3.8: Transition state geometry for addition of nitrone to cyclobutene showing pulling points for both reaction pathways. The hydrogen at the back right of the image is used in both pathways.

As with previous systems under study, we started with the simplest version of the reaction, cycloaddition to cyclobutene. (Figure 3.8) Cyclopropene is not a feasible substrate for

this study as the only possible pulling points would be the hydrogens attached to carbons 1 and 2, which would lead to a reaction barrier dominated by bond stretching, similar to that seen for ethene. Cyclobutene, however, has several available sets of pulling points. For straight-chain alkenes, the choice of pulling points is intuitive; the terminal atoms make the most sensible pulling points. For ring systems, many sets of pulling points are available, and choosing the best set is not intuitive. In choosing between the available sets, the following algorithm was used: For each pair of atoms which could serve as pulling points, the distance between the points was calculated in both reactant and transition state, and the difference in these distances was determined. This quantity corresponds to Δx in Eq. 2. As noted above, if this quantity is positive, one anticipates a decrease in the reaction barrier. If this quantity is negative, an increase in barrier is expected. To achieve the largest effects, the set of pulling points that yielded the largest Δx was used in the subsequent calculations. In the case of ring substrates, it was generally observed that the pulling points leading to the largest negative Δx were located on the same face of the ring as the approaching nitrone molecule, and the largest negative Δx was obtained from pulling points located on the opposite face. For this reason, we have studied multiple reaction pathways for each ring substrate. The pulling points chosen for the reaction with cyclobutene are indicated in Figure 3.8. The combination of nitrone addition to both sides of the ring and pulling from the same face as the nitrone or the opposite face gives rise to a maximum of four reaction pathways. However, many of the rings studied in the thesis, including cyclobutene, display symmetry such that both sides are equivalent for addition. This gives rise to two unique reaction pathways, based on whether pulling points are on the same or opposite sides of the ring from the nitrone addition.

The calculated barriers as a function of applied force are shown in Figure 3.9 for both reaction pathways considered. Clearly, when the pulling points are on the same side of the ring as the nitrone, there is a reduction in the barrier with increasing *F*. The opposite effect is observed when the pulling points and nitrone are on opposite sides of the ring. These trends can be explained using steric effects. When pulling from the same side of ring, denoted pathway 1 in Figure 3.9, steric effects decrease as the top side hydrogen is pulled aside; when pulling from the other side, denoted pathway 2, the bottom hydrogen becoming more equatorial results in the top side hydrogen becoming more axial, which increases steric hindrance to the reaction. It can be seen that these effects are both very small, but going to larger rings should see larger effects, since hydrogen atoms do not contribute much to steric effects but adding more carbons will affect the energetics of the reaction.

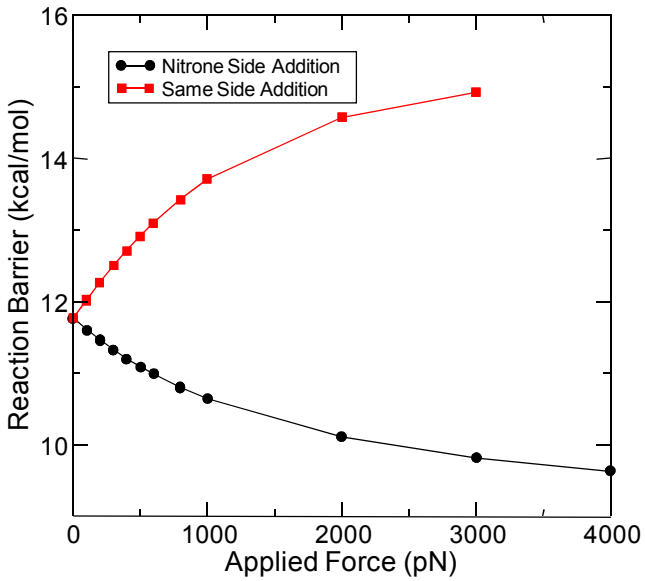

Figure 3.9: Barrier vs force curves for both cyclobutene pathways. Pulling from the same side of the ring as the nitrone addition leads to a reduction of steric hindrance from the hydrogen atoms and reduces the barrier. Pulling from the opposite side moves the hydrogens on that side towards equatorial positions and the hydrogens on the addition side towards axial positions, thus increasing the steric effects and the barrier to reaction.

From cyclobutene it makes sense to move to cyclopentene. The transition state for this reaction with the chosen pulling points indicated is shown in Figure 3.10. Of interest in moving to this larger ring system is that the choice of pulling points becomes somewhat more intuitive; the algorithm described above is still used, but the pulling points chosen are those which are located across the ring from each other, as seen in Figure 3.10. It should be noted that the DOFs affected are analogous to those used in pulling from the terminal methyl groups in hexene, D_{12}, D_{23}, D_{34}, θ_{123}, θ_{234} and φ_{1234}. Again, D_{12} represents the C-C double bond. Unlike the straight-chain alkene substrates, the differences in the shapes of these curves cannot be explained by changing reactant geometry to resemble transition state geometry. Looking at the DOFs affected for each substrate, we ignore those bonds, angles and torsions which are not located between the pulling points on the same end of the ring as the scissile bond. DOFs on the other end of the ring are not significant to the reaction. Thus, stretching from the hydrogen pulling points of cyclopentene affects the same DOFs as stretching from the terminal carbons of straight-chain hexene. The induced geometry changes applying force across these two substrates should be similar, and any difference in the shape of the barrier versus *F* curves must be attributed to another source. In this case, it is hypothesized to be a steric effect, like the changes observed in cyclobutene. This is discussed further in section VII.

Cyclopentene is not symmetric with respect to nitrone addition due to the presence of a "kinked" methylene group, which is not coplanar with the other carbons of the ring, and this combined with same-side and opposite-side pulling points gives four different reaction pathways which can be observed. The barrier-force curves are shown in Figure 3.11. Pathways 2 and 3 refer to the two pathways which use the pulling points on the same side of the ring as the kinked methylene group. Both of these pathways show very small barrier changes, with pathway 2

being the pathway which reduces the steric effects and sees a decrease in the barrier. Pathways 1 and 4 represent pulling from the other side of the ring, and these pathways show a very interesting effect. Within a very small force range, pathways 1 and 4 convert into pathways 3 and 2, respectively, via a force-induced ring flip. Pathway 1 ring-flips in less than 200 pN, while pathway 4 ring-flips with less than 100 pN of applied force. The presence of this ring flip reduces the magnitude that these barrier changes can reach, but considering the very small force regimes which can be observed for these two pathways, the effects are quite large.

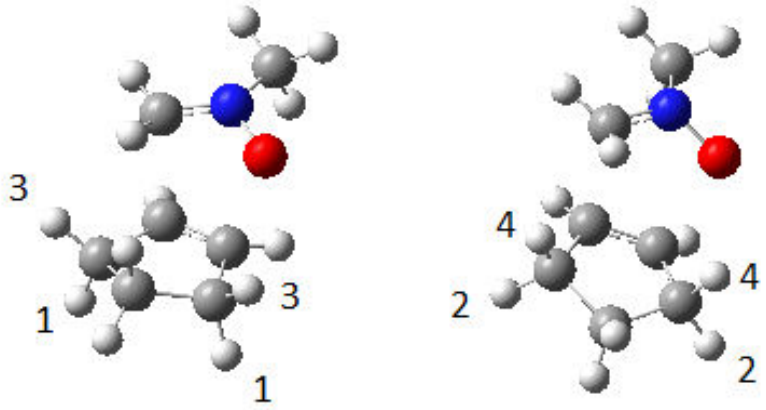

Figure 3.10: Transition state geometries for addition of nitrone to cyclopentene showing pulling points for all four pathways. The left image shows addition to the top of the ring, which is pathways 1 and 3. The right image shows addition to the bottom, and pathways 2 and 4. Pulling points are indicated for each pathway.

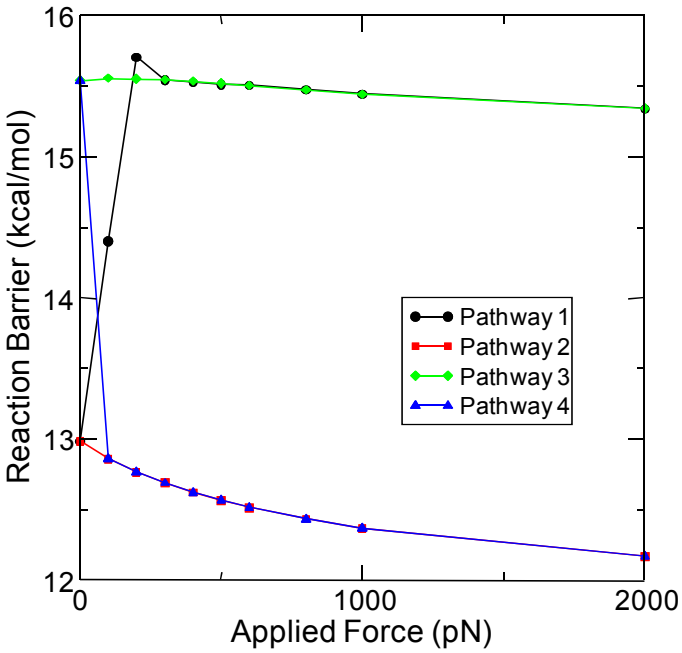

Figure 3.11: Barrier vs force curves for all four cyclopentene pathways.

Continuing on to larger rings, we next investigate addition to cyclohexene. Two distinct pathways exist for this system, depending on whether the nitrone adds to the same face of the ring as the pulling points. The pulling points are analogous to those in straight-chain hexene but the barrier-force curves are different, supporting a steric-based argument as with other ring systems. Figure 3.12 shows the transition state and pulling points, while Figure 3.13 shows the barrier-force curves. Pulling from hydrogens on the same side as the nitrone decreases the barrier due partially to mechanical work effects, including bond stretching and favourable torsion deformation, but also due to a decrease in the steric hindrance from the axial hydrogen atoms. As these are pulled apart, they move away from the nitrone's path of addition and reduce this element of the reaction barrier. The total barrier change is 3.5 kcal/mol over a range of 2500 pN, for a rate constant increase of approximately 1000 times. If the pulling points are on the opposite face of the ring from the nitrone, the opposite effect is seen over small forces: pulling from one

face of the ring forces the methyl groups on the other face to move closer together, further inhibiting nitrone attack at that face. However, this effect does not continue to higher forces, since pulling from this face also induces a flip in the 6-membered ring, such that the methyl groups on the nitrone face are now oriented away from the nitrone, and continued stretching does not result in further barrier increases. This ring flip is shown in Figure 3.14. Due to this, the barrier begins to decrease due to the geometric effects described above for straight-chain hexene, for a total change of 2.5 kcal/mol. It can be seen from this set of simulations that adding geometric constraints in the form of the ring had very little effect on the geometric effects of mechanochemistry, but ring structure offers another means to barrier reduction as the opportunity to mechanochemically affect steric hindrance becomes available. The combination of these two effects leads to a slightly smaller decrease in the barrier than was seen for straight-chain hexene. Thus it can be assumed that the ring system reduces the effects of geometry change, and hydrogen atoms are too small to cause large steric effects. Moving to larger substituents should accentuate the steric component of the barrier change.

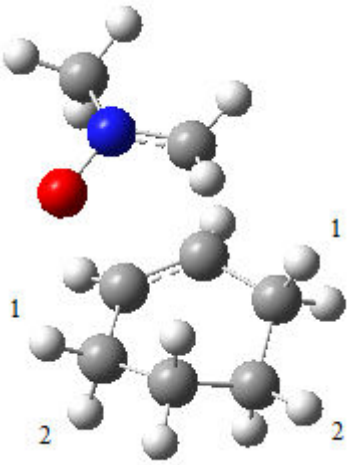

Figure 3.12: Transition state for cycloaddition to cyclohexene. Nitrone side pulling refers to pulling from hydrogens labelled 1, while other side pulling refers to pulling from those labelled 2.

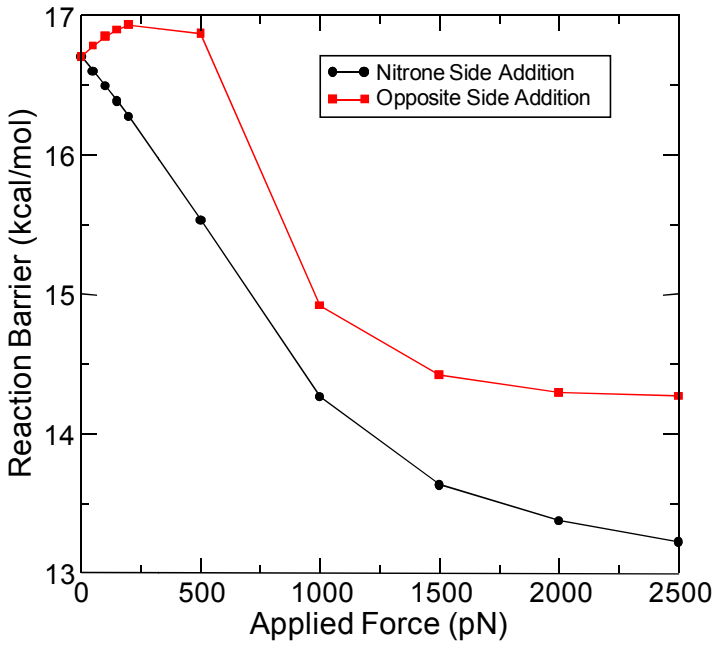

Figure 3.13: Barrier vs force curves for cycloaddition to cyclohexene. Pulling from the nitrone side of the ring reduces steric effects as in cyclobutene for a smooth decrease. Pulling from the other side, however, introduces a maximum to the curve, which is where a ring-flip occurs. The two conformers being interchanged are shown in Figure 3.14. After the ring flip, steric effects begin to decrease with increasing force, and the curve resembles that for nitrone-side pulling.

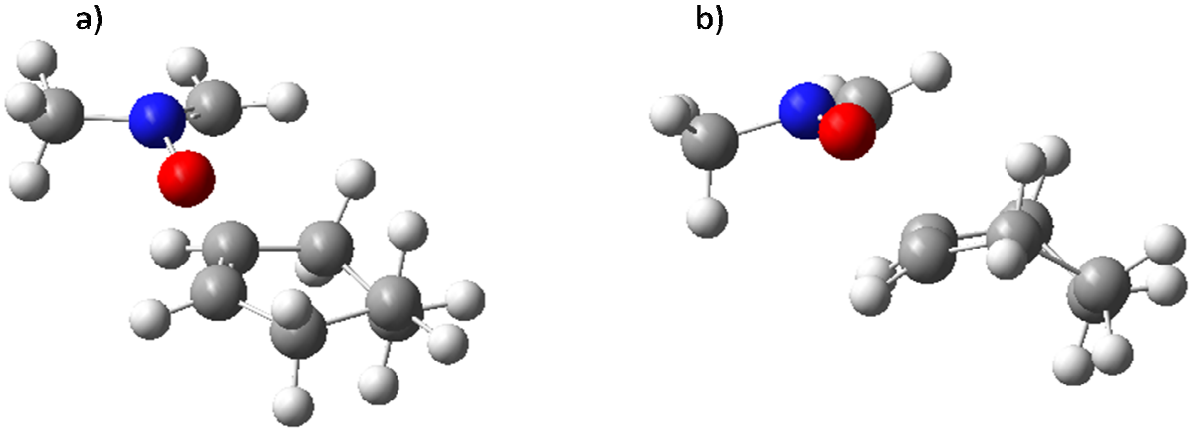

Figure 3.14: Ring flip induced in cyclohexene at 400 pN with the "other side" pulling points. The structure in Figure a) is the initial geometry, which converts to the structure in Figure b) with 400 pN of applied force. It can be seen that after the ring flip the hydrogens on the nitrone side of the ring no longer point directly towards the approaching nitrone, and their steric contribution ceases to hinder the reaction.

VI. Nitrone Cycloaddition to Substituted Cyclic Alkenes

Observing changes in the reaction barrier as a function of force for cyclobutene, cyclopentene and cyclohexene reveals that with these cyclic alkene substrates, steric effects make up a large part of the barrier change, in addition to mechanical work. Having discovered this, we propose that these steric components should increase in magnitude using a more highly-substituted ring as a substrate. This also improves the realism of the reaction since molecular "handles" would be required to perform this reaction experimentally, so calculations on substrates with some kind of hydrocarbon substituent would be more valuable.

The ring system we chose was 3,3,6,6-tetramethylcyclohexene, referred to as TMCH. The transition state structure for this reaction is shown in Figure 3.15, along with the pulling points chosen. As with other ring systems larger than cyclobutene, the DOFs affected are analogous to those of 3-hexene, though the similarity is greater for these systems as all bonds involved are carbon-carbon instead of carbon-hydrogen. Figure 3.16 shows the changes in the reaction barriers with increasing *F* for each reactive system.

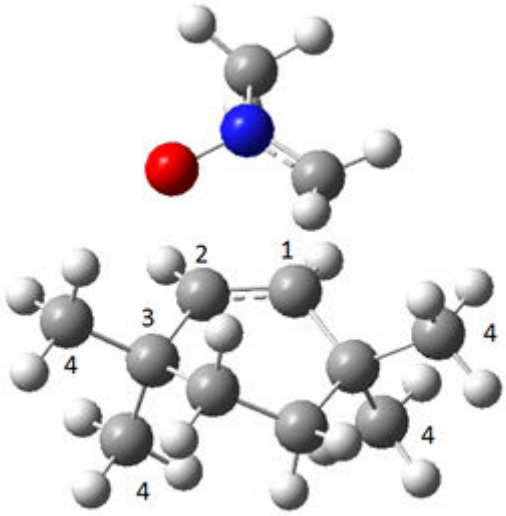

Figure 3.15: Transition states for the Huisgen reaction using TMCH as a substrate. Pulling points are the carbons labelled 4. Using these pulling points allows us to observe changes in DOFs D_{12}, D_{23}, D_{34}, θ_{123}, θ_{234} and φ_{1234}, which are analogous to those in hexene.

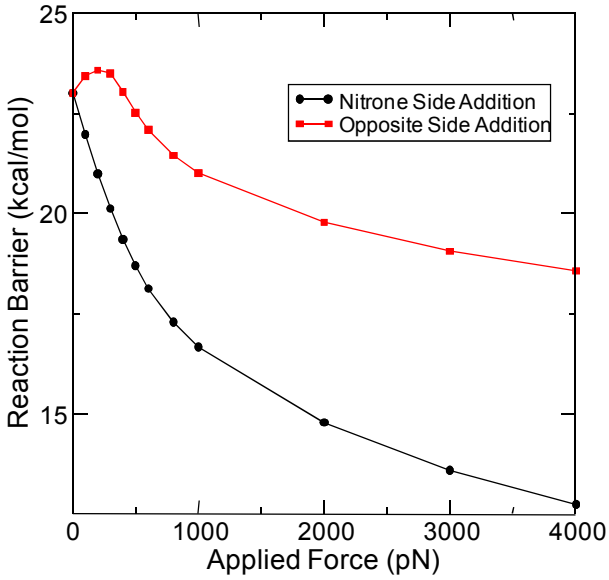

Figure 3.16: Barrier vs Force curves for Huisgen reactions with TMCH substrate. When pulling points are on the same face as the approaching nitrone, a strong barrier reduction is seen as steric resistance and geometric resistance are both overcome by mechanical assistance. When pulling from the opposite face, force works to reinforce steric effects at low force, increasing the barrier. At higher forces, the geometry of the ring changes, switching to a system where sterics are less relevant and so the force results in a reduction of the barrier due to geometric contributions.

It should be noted that the shapes of the curves in Figure 3.16 are very similar to those obtained in the calculations of unsubstituted cyclohexene. As such, it is assumed that the geometric effects are mostly unchanged in going to the larger system. However, the steric effects should be greatly magnified in moving from hydrogen atom pulling points to methyl groups. This seems to be the case, as pulling from the methyl groups in TMCH leads to a barrier change which is much greater than that seen for straight-chain hexene, at least when pulling from the same side of the ring as the nitrone, which is the reaction pathway with the most direct steric effects. Here we observe a barrier change of 10 kcal/mol, corresponding to approximately 10 orders of magnitude of rate increase within the context of transition state theory. Pulling from the opposite side, the barrier-force curve shows the same increase-decrease pattern seen for the same pulling points in cyclohexene, and the observed geometries show the same kind of ring-flip. Again, the barrier changes are greater in magnitude, 4.5 kcal/mol, which can be attributed to the greater steric effects of using the larger ring system.

From the TMCH results, we conclude that sterics play a large role in barrier reductions, thus the logical conclusion of this line of research is to move from TMCH to even more sterically-hindered systems. The next logical step in the progression we have been following would be to study a cyclohexene ring functionalized with t-butyl groups. However, some initial calculations showed this to not be feasible. This system proved too large to perform frequency calculations at the appropriate level of theory to characterize the transition state structure with our modified version of NWCHEM. Because of this, in order to locate and then characterize transition states we would need to move to a new QC code that can perform frequency calculations on large systems, such as Gaussian or GAMESS, which would then require the implementation and testing of our EFEI code into the new software.

VII. Division of Reaction Barrier Changes Into Work and Born-Oppenheimer Terms

In studying barrier changes in ring systems, we conclude that modification of steric interactions is a very important element of altering reaction barriers with mechanochemistry. From the EFEI formalism described above, the barrier changes are due to the combination of mechanical work and Born-Oppenheimer energy. Since most geometric features contributing to the steric interactions being affected in the molecules studied in section VI above do not lie between the pulling points, changes in Δx do not affect them and thus steric effects are not included in the Fx term. Thus, the Born-Oppenheimer energy plays a large role in barrier changes in highly-substituted systems. This is contrary to many theories of mechanochemistry which have been relied on previously, including Bell's model (equation 15 in Chapter II). Since the Born-Oppenheimer energy is calculated based on the geometry of the system, it follows naturally that this value would change when the geometry of the molecule changes under an external force, especially if the force is known to be affecting interatomic interactions such as sterics. If these changes are not equal in magnitude in the transition state and reactant, there will be a change in the Born-Oppenheimer component of the reaction barrier. To study this effect, the work term was calculated as a function of applied force for various Huisgen reactions, and compared to the Born-Oppenheimer component which is equal to the total energy minus the work.

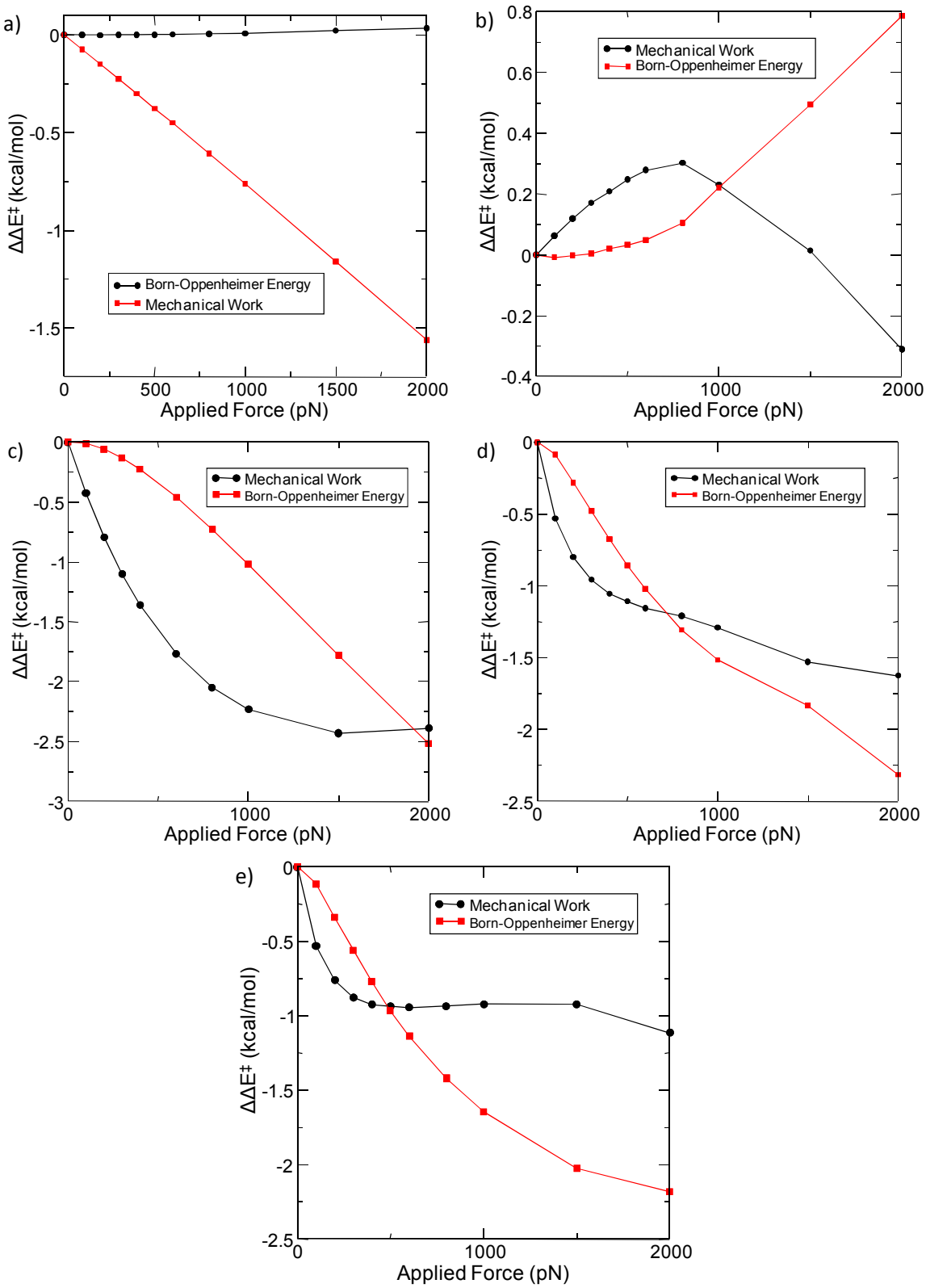

Figure 3.17: Energy-division curves for Huisgen reactions involving straight-chain alkenes. The substrates are: a) Ethene, b) 2-butene, c) 3-hexene, d) 4-octene, e) 5-decene.

Figure 3.17 depicts the results of these energy-division calculations for straight-chain alkenes including ethene, 2-butene, 3-hexene, 4-octene and 5-decene. The differing curves seen in these plots can be explained based on the combination of mechanical and steric effects as discussed in the preceding sections. In the case of ethene, the entire contribution to the barrier reduction is due to mechanical work, arising from extension of the carbon-carbon double bond. The Born-Oppenheimer PESs for reactant and product change very little with increasing force. Butene shows a very different set of effects. As mentioned above, the barrier increases at low forces due to increasing bond angles, which should be seen to decrease in going from reactants to transition state. This effect is overcome by barrier reduction due to bond extension at higher forces. Also at higher forces a steric effect begins to arise as the extension of the terminal methyl groups results in them being brought into closer proximity to the approaching nitrone molecule.

From the data shown in Figure 3.3, it is clear that the remaining three straight-chain alkene substrates show a similar shape for the total barrier vs force curves, and this trend continues into the energy-division curves. Hexene, octene and decene all show a steady decrease in the barrier due to Born-Oppenheimer energy contributions. The mechanical work component of the barrier change shows more interesting behaviour, with a strong initial decrease in the barrier which diminishes until the rate of barrier change with increasing force becomes zero. As explained above, this initial decrease is due to changes in bond lengths and torsions, but the energy division calculations indicate that this effect does not continue past a certain force value. After this point, the rates of geometry change in transition state and reactants become constant, so further changes to the applied force affects the energies of these molecules, but not the reaction barrier. The changes in Born-Oppenheimer energy continue with increasing force, and

this is what causes the barrier to decrease even as the rate of change decreases due to the reduced effect from the mechanical work component. It can be noted that there seems to be a length dependent effect dictating at what point this "levelling-off" of the mechanical component occurs, with the crossing point for the two energy-divided curves moving to lower forces with increasing chain length.

It can be seen that the change in BO energy is similar in magnitude to *Fx* in most of these systems, which is contrary to many assumptions made in the kinetic and energetic discriptions of mechanochemical processes. The large initial decrease in the reaction barrier seen for hexene, octene and decene substrates is based on both components of the energy resulting in a barrier decrease, but the curve begins to level off at higher forces and this can be seen to be due to the work component, while the BO component continues to decrease. It is important to note that both components have the same sign; this indicates that the application of force is moving the system towards the transition state. The *Fx* component should always be negative, but a positive value of the BO energy change indicates that the geometry changes are not moving along the reaction coordinate.

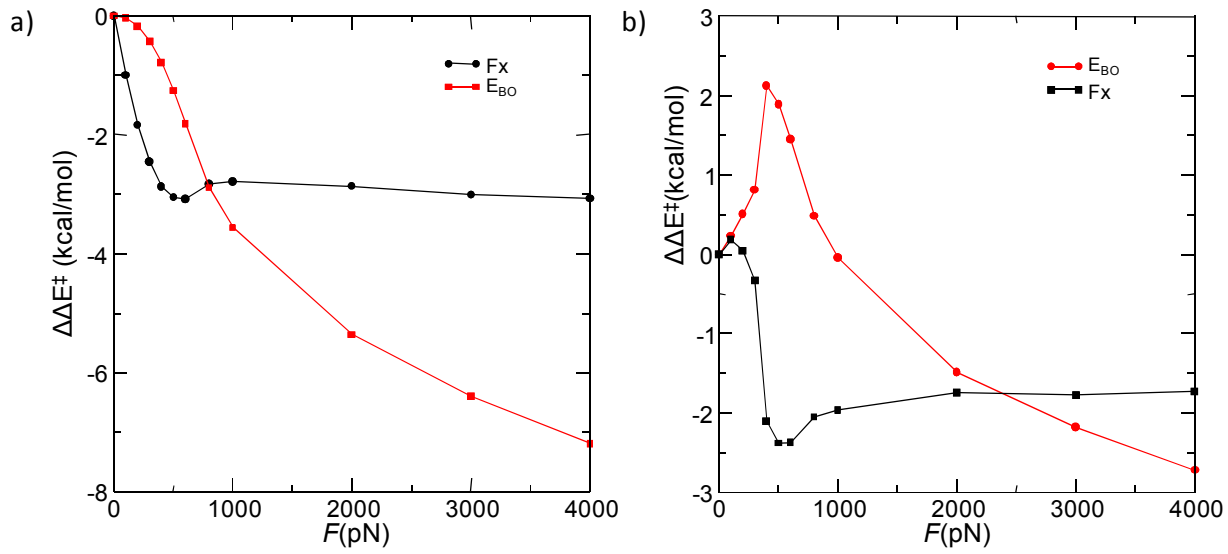

Figure 3.18: Energy division curves for addition to TMCH. Figure a) shows the curves for pulling from the nitrone side of the ring, while Figure b) shows those for pulling from the opposite side.

Different effects are seen from the energy-division of tetramethylcyclohexene. The two pathways seen for this reaction have very different barrier-force curves, and the energy-division analysis shows why. When pulling from the top of the ring, both the BO energy and the work term cause a decrease in the barrier, which leads to the very pronounced barrier change of nearly 10 kcal/mol. Pulling from the other side, however, the BO energy prior to the ring flip shows a very strong opposition to the force, leading to the maximum seen at 100-300 pN in the barrier-force curve. At low forces, the geometry is moved towards reactants rather than towards the transition state, and the barrier increases. At approximately 400 pN of force, the ring flip occurs and these effects disappear. In both reaction pathways, above 1 nN of force, the work component of the energy is seen to level off. This does not indicate that the work term has stopped acting upon the system, only that it is equivalent in reactant and transition state and thus has no effect on the barriers. Continued reduction of the barrier is at this point based solely on changes in the Born-Oppenheimer energy induced by the mechanical force. From this, we can

state that the energetic and kinetic models stated in equations (1) and (2) are not adequate descriptions of mechanochemically-affected reactions. In the Arrhenius and Bell[58] models, both the Born-Oppenheimer energy E_{BO} and the extension Δx are defined as being unchanged when stress is applied, and only the value of F changes. This is clearly false from the energy-division results presented here. In the Marx model,[37] a changing value of Δx and E_{BO} are not implied, but can be readily incorporated simply by using the appropriate values. This is what must be done to achieve a proper energetic description of a reaction under the influence of mechanical force.

Chapter 4: Conclusions and Future Work

We have chosen to study the little-examined area of bimolecular reactions under mechanochemical conditions. Specifically, we have investigated the effects of applied force of magnitude below the bond-stretching regime to 1,3-dipolar cycloadditions of N-methyl nitrone to alkene substrates. We performed quantum chemical calculations at the B3LYP/6-31G** level of theory with the EFEI method of force modification to locate minima and transition states (TSs) on a force-modified potential energy surface to obtain reaction barriers for these reactions. Barriers were obtained over a range of forces for several different alkene-containing substrates, and from this we have obtained a better understanding of how applied force changes these reactions.

Previous studies have shown that applied force modifies the geometry of reactants and TSs such that a barrier change occurs.[21, 34, 47] If the application of external force induces geometry changes which cause the Born-Oppenheimer energy of the reactant and TS to move closer together, a barrier decrease will result, and if the difference in these energies grows larger, the barrier will increase. In terms of specific geometry changes, we have identified that bond-stretching plays a relatively minor role in changing reaction barriers in the low-force regime, and rather it is changes in bond angles and especially torsions which have the largest effect.

In addition to identifying the DOFs responsible for the largest parts of barrier change, we have also identified additional effects that lead to large barrier changes. In the EFEI formalism, barrier changes are attributed to both mechanical work and changes in the energy of the Born-Oppenheimer PES. E_{BO} changes follow logically since the PES is force-modified, but the largest E_{BO} changes are associated with modification of steric effects. Thus, the largest barrier reductions we observe were from systems with significant angle and torsion changes that make

the reactant structure more TS-like and also include large steric effects which can be decreased through the application of force. These were seen in ring systems, where the constraint of the ring intensifies barrier changes due to geometric effects, and especially in ring systems with large substituents, which lead to large steric repulsions which can be reduced by application of force with the proper pulling points.

Our overall goal for this research area is to assist in the development of mechanochemistry as a tool for chemical synthesis. Mechanochemical activation of reactions offers a possible method for reducing the time frames required for certain reactions, and can lead to mechanoselectivity, providing new avenues for accessing unfavoured reaction pathways. In order for this sort of practical application to become a reality, certain goals must be achieved, some of which have been furthered in this thesis. We require an understanding of what elements are necessary for a strong mechanical activation of a reaction, a mathematical method for predicting the magnitude of this barrier change, and most importantly a practical method of applying external force in the laboratory setting. Of these three, we have made progress towards the first of these goals, though the second requires much further study, and the third is beyond the scope of our research, although recent results from Boulatov show great promise.[47]

Based on the results presented in this thesis, we have reached a much greater understanding of the geometric elements of mechanical activation. However, there is still a great deal of room for investigation of reactions and/or substrates which lead to significant barrier changes. The issues involved in simulating large substituted ring systems, as we discovered with t-butyl-substituted cyclohexene, indicate that it would be wise to study a wider range of reactions involving small or at least easily-modeled molecules. We have also identified the importance of angle and torsion deformations in contributing to these effects, as well as the role of sterics.

Thus, in searching for new reactions for study under mechanochemical conditions it would be valuable to search for reactions where there are large changes in angles and torsions in moving from reactant to transition state, and significant steric hindrance to reaction. Such a reaction would present opportunities for significant barrier reduction through both mechanical work and E_{BO} modification, so this is the sort of reactant structure we would look for in searching for new mechanically-active reactions, and looking into a range of such reactions would further our understanding of mechanochemical activation.

The energetics and kinetics of mechanically-activated reactions are not well understood, and this presents another area ripe for further study. For any area of chemistry that seeks to alter reaction barriers and thereby reaction rates, an understanding of exactly how barrier changes lead to rate changes is important. Also relevant to development of practical mechanochemistry is the need for a predictive model, whereby some estimate as to the barrier change that a reaction will undergo can be obtained without performing extensive calculations. The most popular semi-predictive model available at this point is Bell's model,[54] since the value of F is known beforehand and the value of x can be calculated based on the reactant and transition state structures at F=0 pN. However, this model does not allow for changes in E_{BO}, and we have observed from our energy-division calculations that this cannot be ignored. Changes in E_{BO} are much more difficult to predict than changes in Fx, but if they could be predicted then many time-consuming computational steps could be avoided. A first attempt at estimating barrier changes was suggested by the Mosey group, and is given in equation 22:

$$\Delta E^{\ddagger} = E_0^{\ddagger} - F\Delta x - \frac{F^2}{2}\left(\frac{1}{k_{TS}} - \frac{1}{k_r}\right) \qquad (22)$$

This equation represents a second-order expansion of Bell's model, and assumes harmonic behaviour in terms of the E_{BO} change, describing that with the third term. In this equation, k_{ts}

and k_r represent effective force constants for the transition state and reactant geometries respectively. The equation has two weaknesses: First, a small number of calculations must be performed in order to estimate these effective force constants, and second, this model does not always work at larger forces. In a system where a harmonic approximation is valid to high forces, this equation will be useful over a large range. This harmonic description for E_{BO} change is appropriate in the low-force region for most systems, but once significant angle and torsion deformations that induce large changes in structure begin to appear, this model loses effectiveness quickly. Thus, a second-order harmonic approximation is not satisfactory as a predictive model for most systems, and further experimentation will be required to understand the factors which go into barrier changes from a quantitative perspective. The investigation of these factors, and development of predictive models for the effects of applied stress on reaction barriers will be the focus of future research.

References

(1) Beyer, M. K.; Clausen-Schaumann, H. *Chem. Rev.* **2005***, 105*, 2921.

(2) Fersht, A. In *Enzyme Structure and Mechanism;* 1985; Vol. xxi, 475.

(3) Boldyrev, V. V.; Tkacova, K. *J. Mat. Syn. Proc.* **2000***, 8*, 121.

(4) Pike, M.; Watson, W. F. *J. Polymer Sci.* **1952***, 9*, 229.

(5) Ayrey, G.; Moore, C. G.; Watson, W. F. *J. Polymer Sci.* **1956***, 19*, 1.

(6) Mitchenko, S. A.; Khomutov, E. V.; Kovalenko, V. V.; Popov, A. F.; Beletskaya, I. P. *Inorg. Chim. Act.* **2001***, 320*, 31.

(7) Kameda, J.; Saruwatari, K.; Tanaka, H. *J. Colloid Interface Sci.* **2004***, 275*, 225.

(8) Watson, W. F. *Makromol. Chem.* **1959***, 6*, 1508.

(9) Heegn, H. *Chem. Ing. Technol.* **2001***, 73*, 1529.

(10) Walter, N. G.; Huang, C. -Y.; Manzo, A. J.; Sobhy, M. A. *Nature Methods* **2008***, 5*, 475.

(11) Ando, T.; Kodera, N.; Takai, E.; Maruyama, D.; Saito, K.; Toda, A. *Proc. Natl. Acad. Sci. USA* **2001***, 98*, 12468.

(12) Block, S. M.; Neuman, K. C. *Rev. Sci. Instrum.* **2004***, 75*, 2788.

(13) Neuman, K. C.; Nagy, A. *Nature Methods* **2008***, 5*, 491.

(14) Xiang, Y.; Morais, M. C.; Battisti, A. J.; Grimes, S.; Jardine, P. J.; Anderson, P. L.; Rossman, M. G. *Embo Journal* **2006***, 25*, 5229.

(15) Greenberg, M. J.; Moore, J. R. *Cytoskeleton* **2010***, 67*, 273.

(16) deCastro, M. J.; Fondecave, R. M.; Clarke, L. A.; Schmidt, C. F.; Stewart, R. J. *Nature Cell. Bio.* **2000***, 2*, 724.

(17) Croquette, V.; Mosconi, F.; Allemand, J. F.; Bensimon, D. *Phys. Rev. Lett.* **2009***, 102*, 078301.

(18) Finzi, L.; Dunlap, D. D. *J. Bio. Chem.* **2010***, 285*, 18973.

(19) Ranzoni, A.; Janssen, X. J. A.; Ovsyanko, M.; van IJzendoorn, L. J.; Prins, L. W. J. *Lab on a Chip* **2010***, 10*, 179.

(20) Boldyrev, V. V. *Ultrason. Sonochem.* **1995***, 2*, S143.

(21) Boulatov, R.; Yang, Q. -Z.; Huang, Z.; Kucharski, T. J.; Khvostichenko, D.; Chen, K. *Nature Nanotech.* **2009**, *4*, 302.

(22) Hickenboth, H. R.; Moore, J. S.; White, S. R.; Sottos, N. R.; Baudry, J.; Wilson, S. R. *Nature* **2007***, 446*, 423.

(23) Zhurkov, S. N.; Tomashevskii, E. E.; Savostin, A. Y. *Doki. Akad. Nauk S. S. S. R.* **1964***, 159*, 303.

(24) Zhurkov, S. N.; Korsukov, V. E. J. *J. Polym. Sci. B* **1974***, 12*, 385.

(25) Porter, R. S.; Johnson, J. F. J. *J. Phys. Chem.* **1959***, 63*, 202.

(26) Grandbois, M.; Beyer, M.; Clausen-Schaumann, H.; Gaub, H. E. *Science* **1999***, 283*, 1727.

(27) Kruger, D.; Rousseau, R.; Fuchs, H.; Marx, D. *Angew. Chem. Int. Ed.* **2001***, 42*, 2251.

(28) Rubio, G.; Agrait, N.; Vieira, S. *Phys. Rev. Lett.* **1996***, 76*, 2302.

(29) Rubio-Bollinger, G.; Bahn, S. R.; Agrait, N.; Jacobeen, K. W.; Vieira, S. *Phys. Rev. Lett.* **2001***, 87*, 026101.

(30) Kruger, D.; Rousseau, R.; Fuchs, H.; Marx, D. *Angew. Chem. Int. Ed.* **2003***, 42*, 2251.

(31) Beyer, M. K. *J. Chem. Phys.* **2000***, 112*, 7307.

(32) Aktah, D.; Frank, I. *J. Am. Chem. Soc.* **2001***, 124*, 3402.

(33) Wiita, P. W.; Ainavarapu, S. R. K.; Huang, H. H.; Fernandez, J. M. *Proc. Nat. Acad. Sci.* **2006***, 103*, 7222.

(34) Beyer, M. K. *Angew. Chem. Int. Ed.* **2003***, 42*, 4913.

(35) Rohrig, U. F.; Frank, I. *J. Chem. Phys* **2001***, 115*, 8670.

(36) Martinez, T. J.; Virshup, A. M.; Tao, H.; Leiding, J.; Ong, M. T. *J. Am. Chem. Soc.* **2009**, *131*, 6377.

(37) Ribas-Arino, J.; Shiga, M.; Marx, D. *Angew. Chem. Int. Ed.* **2009***, 48*, 4190.

(38) Kochhar, G. S.; Bailey, A.; Mosey, N. J. *Angew. Chem. Int. Ed.* **2010***, 49*, 7452.

(39) Popov, A. A.; Krisyuk, B. E.; Blinov, N. N.; Zaikov, G. E. *Eur. Polym. J.* **1981***, 17*, 169.

(40) Popov, A. A.; Krisyuk, B. E.; Zaikov, G. E. *Vysokomol. Soedin. Ser. A* **1980***, 22*, 329.

(41) Bershtein, V. A.; Egorova, L. M. *Vysokomol. Soedin. Ser. Ako* **1977***, 19*, 1260.

(42) Rapoport, N. Y.; Livanova, N. M.; Grigorev, A. G.; Zaikov, G. Y. *Vysokomol. Soedin. Ser. A* **1983***, 25*, 2188.

(43) Rapoport, N. Y.; Zaikov, G. Y. *Usp. Khim.* **1983***, 52*, 1568.

(44) Dymova, T. N.; Konoplev, V. N.; Sizareva, A. S.; Aleksandrov, D. P. *Russ. J. Coord. Chem.* **2000***, 26*, 531.

(45) Valiev, M.; Bylaska, E. J.; Govind, N.; Kowalski, K.; Straatsma, T. P.; van Dam, H. J. J.; Wang, D.; Nieplocha, J.; Apra, E.; Windus, T. L.; de Jong, W. A. *Comput. Phys. Commun.* **2010***, 181*, 1477.

(46) Giannozzi, P.; et al *J. Phys. Condens. Matt.* **2009***, 21*, 395502.

(47) Boulatov, R.; Huang, Z.; Yang, Q. -Z.; Khvostichenko, D.; Kucharski, T. J.; Chen, J. *J. Am. Chem. Soc.* **2009***, 131*, 1407.

(48) Hehre, W. J.; Radom, L.; Pople, J. A.; Schleyer, P. v. R. In *Ab initio Molecular Orbital Theory;* McGraw-Hill: New York, 1987.

(49) Kohn, W.; Sham, L. *J. Phys. Rev.* **1965***, 140*, A1133.

(50) Perdew, J. P.; Wang, Y. *Phys. Rev. B* **1992***, 45*, 13244.

(51) Koch, W.; Holthausen, M. C. In *A Chemist's Guide to Density Functional Theory.* Wiley-VCH: Weinham, 2001.

(52) Vosko, S. J.; Wilk, L.; Nusair, M. *Can. J. Phys.* **1980***, 58*, 1200.

(53) Becke, A. D. *J. Chem. Phys.* **1993***, 98*, 5648.

(54) Lee, C.; Yang, W.; Parr, R. G. *Phys. Rev. B* **1988***, 37*, 785.

(55) Ditchfield, R.; Hehre, W. J.; Pople, J. A. *J. Chem. Phys.* **1974***, 54*, 724.

(56) Zhurkov, S. N. *Intern. J. Fracture Mech.* **1965***, 1*, 311.

(57) Zhurkov, S. N.; Narzullaev, B. N. *Zh. Tekh. Fiz.* **1953***, 23*, 1677.

(58) Bell, G. I. *Science* **1978***, 200*, 618.

(59) Laidler, K.; King, C. *J. Phys. Chem.* **1983***, 87*, 2657.

(60) Di Valentin, C.; Freccero, M.; Gandolfi, R.; Rastelli, A. *J. Org. Chem.* **2000***, 65*, 6112.

(61) Loh, B.; Vozzolo, L.; Mok, B. J.; Lee, C. C.; Fitzmaurice, R. J.; Caddick, S.; Fassati, A. *Chem. Biol. Drug. Des.* **2010***, 75*, 461.

(62) Swift, P. A.; Mullen, G. B.; Mitchell, J. T.; Allen, S. D.; StGeorgiev, V. *Chemotherapy* **1989***, 35*, 130.

(63) Russak, J. A.; Carrillo, N. *Ab. Pap. Am. Chem. Soc.* **2008***, 236*, 366.

(64) Damodiran, M.; Sivakumar, P. M.; SenthilKumar, R.; Muralidharan, D.; Kumar, B. V. N. P.; Doble, M.; Perumal, P. T. *Chem. Biol. Drug Des.* **2009***, 74*, 494.

(65) Ribas-Arino, J.; Shiga, M.; Marx, D. *J. Am. Chem. Soc.* **2010**, *132*, 10609.